Q. J. R. Meteorol. Soc. (1999), **125**, pp. 301–330

Accounting for subgrid-scale cloud variability in a multi-layer 1D solar radiative transfer algorithm

By LAZAROS OREOPOULOS and HOWARD W. BARKER*†
Atmospheric Environment Service, Canada

(Received 22 July 1997; revised 26 February 1998)

SUMMARY

A multi-layer, 1D solar radiative transfer algorithm that accounts for subgrid-scale cloud variability is presented. This algorithm is efficient and suitable for use in large-scale models such as global climate and weather prediction models. While it is built on the same principles as standard multi-layer 1D codes, there are two major differences. First, it is assumed that for all cloudy layers all the time, frequency distributions of optical depth τ are described by gamma probability density functions $p_\Gamma(\tau)$ and characterized by mean optical depth $\bar{\tau}$ and a variance-related parameter ν. Albedos and transmittances for individual layers are estimated by integrals over all τ of the plane-parallel, homogeneous two-stream approximation equations weighted by $p_\Gamma(\tau)$. Thus, the model is referred to as the gamma-weighted two-stream approximation. Second, in an attempt to counteract the use of horizontally homogeneous fluxes, a method was devised that often reduces layer values of $\bar{\tau}$.

The gamma-weighted two-stream approximation was implemented in a well known broadband column model and the parametrizations upon which it is built were tested using 2D and 3D inhomogeneous cloud fields generated by a bounded cascade model and cloud-resolving models. All fields resolved the lowest 20 km of the atmosphere into at least 30 layers. Reference calculations were obtained by: (i) applying the 1D-plane-parallel, homogeneous model to each column and averaging (the independent column approximation); and (ii) a 3D Monte Carlo algorithm. The gamma-weighted two-stream approximation, the regular plane-parallel, homogeneous, and two other 1D models operated on horizontally-averaged versions of the fields (i.e. 1D vectors of cloud fraction, $\bar{\tau}$, and ν). For several demanding cases, the gamma-weighted two-stream approximation reduced plane-parallel, homogeneous-biases for TOA albedo and surface irradiance by typically more than 85%. Moreover, its estimates of atmospheric heating rates usually differed from the independent column approximation and Monte Carlo values by less than 10%. This translates into heating rate errors that are four to eight times smaller than those associated with conventional 1D plane-parallel, homogeneous algorithms. In a large-scale model, a multi-layer solar code with the gamma-weighted two-stream approximation should require about twice as much CPU time as its plane-parallel, homogeneous counterpart.

KEYWORDS: Inhomogeneity Parametrization Solar radiation

1. INTRODUCTION

Large-scale models (LSMs) of the atmosphere used to study climate and weather operate with horizontal grid-spacings of typically ~50 km to ~500 km. For most cases, therefore, it is adequate to assume that grid-averaged solar radiative fluxes can be computed accurately by treating multi-layer columns in isolation. Hence, much work went, and continues to go, into development of 1D plane-parallel, homogeneous (PPH) algorithms (e.g. Wiscombe 1977; Fouquart and Bonnel 1980; Chou 1992; Briegleb 1992; Edwards and Slingo 1996). At these grid-spacings, however, it is inadequate to assume, as do 1D-PPH models, that subgrid-scale cloud optical properties lack horizontal variability. For example, it has long been recognized that fractional cloud amounts are important for making accurate flux estimates (Schneider and Dickinson 1976), but accounting for this in multi-layer 1D models has ambiguities (Morcrette and Fouquart 1986). More generally, several studies have demonstrated that neglect of horizontal variations in cloud optical depth τ imparts sizable biases on estimated solar fluxes (e.g. Stephens 1988a,b; Cahalan *et al.* 1994a; Barker 1996; Barker *et al.* 1998; Oreopoulos and Davies 1998a). Since 1D models represent the only viable means of computing solar fluxes and heating rates in LSMs, there is a need to develop tractable and accurate algorithms capable of handling descriptions of subgrid-scale cloud variability.

* Corresponding author: Atmospheric Environment Service, Cloud Physics Research Division (ARMP), 4905 Dufferin Street, Downsview, ON, Canada M3H 5T4. e-mail: howard.barker@ec.gc.ca
† Additional affiliation: Department of Oceanography, Atmospheric Science Programme, Dalhousie University, Halifax, NS, Canada.

Most, if not all, LSMs employ a two-stream approximation of the radiative transfer equation (Meador and Weaver 1980) to account for multiple-scattering of solar radiation by cloudy atmospheres. In an attempt to address subgrid-scale cloud variability in an LSM, Tiedtke (1996) utilized Cahalan *et al.*'s (1994a) effective thickness approximation (ETA) by passing 0.7τ, where τ is LSM-generated optical depth, to the LSM's delta-Eddington (Joseph *et al.* 1976) subroutine. This approach is similar to Yu *et al.*'s (1997) use of 0.28τ and McFarlane *et al.*'s (1992) use of $\tau^{0.8}$ (Davis *et al.* 1990). However, as discussed by Cahalan *et al.* (1994a) and Barker (1996), simply reducing optical depth passed to a PPH model holds only for a rather narrow range of optical depths and solar zenith angles and could have undesirable effects on estimates of cloud absorptance.

A second, more versatile, approach is to weight the two-stream response functions by a density function $p(\tau)$ and integrate over all τ (Stephens *et al.* 1991). This is essentially an independent column approximation (ICA)*. Use of the gamma distribution to represent $p(\tau)$ is supported by evidence from Landsat imagery of marine boundary layer (MBL) clouds (Barker *et al.* 1996), Advanced Very High Resolution Radiometer (AVHRR) imagery of numerous cloud types (Oreopoulos and Davies 1998b), and cloud-resolving model simulations of both MBL clouds (personal communication, B. Stevens and S. Krueger 1996) and mesoscale convective systems (see Barker *et al.* 1998). The resulting model is referred to hereinafter as the gamma-weighted two-stream approximation (GWTSA). While the GWTSA equations are more tractable than one might expect, they require ~four times more computational effort than the standard two-stream (Barker 1996) as well as an additional variable not provided by current LSMs: mean logarithm or variance of τ.

The objective of the current study was to develop a multi-layer 1D solar radiative transfer code for use in LSMs that uses the GWTSA to account for subgrid-scale cloud variability. This algorithm is developed in the second section. The third section describes models whose results were used to either contrast or assess GWTSA results. In the fourth section, the GWTSA's performance is compared with that of other column models using both idealized 2D fractal-like clouds and 2D and 3D cloud fields derived from cloud-resolving models. Benchmark calculations are provided by the explicit ICA and a 3D Monte Carlo photon transport analog of the 1D column models. A short discussion and concluding comments are made in section five.

2. Model development

(a) *Basic framework*

The new model is applicable to all 1D algorithms that are based on two-stream approximations of the radiative transfer equation. Before discussing its parametrizations, some basic PPH axioms are recapitulated because the new model is built on them. Following Liou's development of the principles of invariance (Liou 1992), albedo and transmittance for a system consisting of two PPH layers irradiated by a collimated beam (onto the top of layer 1) are

$$R_{1,2}(\mu_0) = R_1(\mu_0) + \frac{t_1\{[T_1(\mu_0) - T_1^{\mathrm{dir}}]r_2 + T_1^{\mathrm{dir}}R_2(\mu_0)\}}{1 - r_1 r_2} \tag{1a}$$

* The term *independent column approximation* (ICA) is synonymous with the term *independent pixel approximation* (IPA). Though IPA has been used much in the past (e.g. Cahalan *et al.* 1994b; Barker 1996; Gabriel and Evans 1996), we prefer ICA and feel that IPA should be reserved for satellite imagery and ICA for radiative transfer calculations.

and

$$T_{1,2}(\mu_0) = T_1^{\text{dir}} T_2(\mu_0) + \frac{t_2\{[T_1(\mu_0) - T_1^{\text{dir}}] + T_1^{\text{dir}} R_2(\mu_0) r_1\}}{1 - r_1 r_2} \tag{1b}$$

where $R_i(\mu_0)$ and $T_i(\mu_0)$ are layer albedos and transmittance for direct-beam incident at a solar zenith angle of θ_0 ($= \cos^{-1} \mu_0$), and r_i and t_i are corresponding solutions for a diffuse source. For homogeneous layers, transmittance for direct-beam only is

$$T_1^{\text{dir}} = e^{-\bar{\tau}_1/\mu_o} \tag{2}$$

where $\bar{\tau}_1$ is mean optical depth of the upper layer (scaled for forward-scattering (Wiscombe 1977)). If the source is diffuse irradiance, overall albedo and transmittance are

$$r_{1,2} = r_1 + \frac{t_1^2 r_2}{1 - r_1 r_2}. \tag{3a}$$

and

$$t_{1,2} = \frac{t_1 t_2}{1 - r_1 r_2}. \tag{3b}$$

For a multi-layered atmosphere, passes are made from top-to-bottom and bottom-to-top to build matrices of albedos and transmittances for collections of layers. Then, up and down fluxes at the i^{th} level are computed as

$$F_i^{\uparrow} = \mu_0 S \left\{ \frac{T_{1,i-1}^{\text{dir}} R_{i,N}(\mu_0) + [T_{1,i-1}(\mu_0) - T_{1,i-1}^{\text{dir}}] r_{i,N}}{1 - r_{i-1,1} r_{i,N}} \right\} \tag{4a}$$

and

$$F_i^{\downarrow} = \mu_0 S \left\{ T_{1,i-1}^{\text{dir}} + \frac{T_{1,i-1}^{\text{dir}} R_{i,N}(\mu_0) r_{1,i-1} + [T_{1,i-1}(\mu_0) - T_{1,i-1}^{\text{dir}}]}{1 - r_{i-1,1} r_{i,N}} \right\} \tag{4b}$$

where the top and bottom layers are numbered 1 and N, S is incident solar flux at the TOA,

$$T_{1,i-1}^{\text{dir}} = \prod_{n=1}^{i-1} e^{-\bar{\tau}_n/\mu_0} \tag{5}$$

and the subscript convention means that, for example $r_{i-1,1}$ and $r_{i,N}$ are reflectances for groups of layers between the $(i-1)^{\text{th}}$ layer, and the top layer and the i^{th} layer and the bottom layer to upwelling and downwelling diffuse beams, respectively. The usual practice is to compute R_i, T_i, r_i, and t_i by a standard PPH flux solution to the equation of transfer [see Meador and Weaver (1980) for standardized equations]. This is where the new 1D model diverges from existing models as it attempts to address subgrid-scale cloud variability. Parametrizations used in the new model are presented in the following subsections.

(*b*) *Individual layers*

This subsection describes how R_i, T_i, r_i, and t_i are computed. Most LSMs attempt to diagnose the fraction of a layer occupied by cloud.* Therefore, overall layer values for

* Assume that clouds extend through the depth of layers and that the term *cloud fraction* means vertically-projected cloud fraction (Barker and Wielicki 1997).

use in (4) and (5) are computed as simple linear combinations of clear- and cloudy-sky quantities weighted by their respective fractions (Morcrette and Fouquart 1986). Thus,

$$R_i = (1 - C_i)R_{\mathrm{clr},i} + C_i R_{\mathrm{cld},i} \tag{6a}$$
$$T_i = (1 - C_i)T_{\mathrm{clr},i} + C_i T_{\mathrm{cld},i} \tag{6b}$$
$$r_i = (1 - C_i)r_{\mathrm{clr},i} + C_i r_{\mathrm{cld},i} \tag{6c}$$
$$t_i = (1 - C_i)t_{\mathrm{clr},i} + C_i t_{\mathrm{cld},i} \tag{6d}$$
$$T_i^{\mathrm{dir}} = (1 - C_i)T_{\mathrm{clr},i}^{\mathrm{dir}} + C_i T_{\mathrm{cld},i}^{\mathrm{dir}} \tag{6e}$$

where C_i is cloud fraction in the i^{th} layer, and subscripts clr and cld correspond to clear- and cloudy-sky albedos and transmittances. This represents a type of random overlapping of clouds which carries the assumption of zero correlation between cloud extinction and radiation (see Stephens 1988b). It is easy to show that this differs from the formal random overlap method as used, for example, by Stubenrauch *et al.* (1997). Ideally, the clear-sky components are computed by a PPH two-stream suitable for optically thin layers (e.g. Coakley and Chýlek 1975) using effective values of optical depth τ, single-scattering albedo ω_0, and asymmetry parameter g for mixtures of air molecules (i.e. Rayleigh scattering), absorbing gases, and aerosols:

$$\tau_{\mathrm{clr}} = \tau_{\mathrm{ray}} + \tau_{\mathrm{gas}} + \tau_{\mathrm{aero}} \tag{7a}$$
$$\omega_{\mathrm{clr}} = \frac{\tau_{\mathrm{ray}} + \omega_{\mathrm{aero}}\tau_{\mathrm{aero}}}{\tau_{\mathrm{clr}}} \tag{7b}$$
$$g_{\mathrm{clr}} = \frac{g_{\mathrm{aero}}\omega_{\mathrm{aero}}\tau_{\mathrm{aero}}}{\omega_{\mathrm{clr}}\tau_{\mathrm{clr}}}. \tag{7c}$$

The main point of this section, however, is cloud contributions in (6).

Cahalan *et al.* (1994b) showed that albedo for planar marine boundary layer (MBL) clouds (with horizontal variability of liquid water path $\mathcal{L}$ only) can be computed very accurately by applying a standard PPH two-stream approximation to N columns of optical depth τ_n in a domain $\mathcal{R}$ and averaging. This is the explicit ICA method in which μ_0 dependent values are defined as

$$\left.\begin{matrix} R_{\mathrm{ica}}(\mu_0) \\ T_{\mathrm{ica}}(\mu_0) \end{matrix}\right\} \equiv \frac{1}{N}\sum_{n=1}^{N}\left\{\begin{matrix} R_{\mathrm{pph}}(\mu_0, \tau_n) \\ T_{\mathrm{pph}}(\mu_0, \tau_n) \end{matrix}\right\} \tag{8}$$

where R_{pph} and T_{pph} are PPH two-stream estimates. Solutions for a diffuse source are defined similarly using $r_{\mathrm{pph}}(\tau_n)$ and $t_{\mathrm{pph}}(\tau_n)$.

If $p(\tau)$ is an idealized, normalized, probability density function for τ in $\mathcal{R}$, (8) could be approximated (e.g. Stephens *et al.* 1991) as

$$\left.\begin{matrix} R[\mu_0;\, p(\tau)] \\ T[\mu_0;\, p(\tau)] \end{matrix}\right\} \equiv \int_0^{\infty} p(\tau)\left\{\begin{matrix} R_{\mathrm{pph}}(\mu_0, \tau) \\ T_{\mathrm{pph}}(\mu_0, \tau) \end{matrix}\right\} \mathrm{d}\tau. \tag{9}$$

As mentioned in the Introduction, there is some evidence suggesting that the gamma distribution $p_\Gamma(\tau)$ is often a suitable form for $p(\tau)$. Moreover, Barker *et al.* (1996) demonstrated that even when $p_\Gamma(\tau)$ is only a moderately good approximation to $p(\tau)$, compensating errors usually result in excellent agreement between (8) and (9). Thus, writing

$$p_\Gamma(\tau) = \frac{1}{\Gamma(\nu)}\left(\frac{\nu}{\bar{\tau}}\right)^{\nu} \tau^{\nu-1} e^{-\nu\tau/\bar{\tau}}; \quad [\nu > 0,\ \bar{\tau} > 0] \tag{10}$$

where $\Gamma(\nu)$ is the gamma function and $\bar{\tau}$ is mean optical depth, it is recommended that ν be determined by maximum likelihood estimation (MLE) by solving

$$\frac{\mathrm{d}}{\mathrm{d}\nu} \ln \Gamma(\nu) + \ln\left(\frac{\bar{\tau}}{\nu}\right) - \overline{\ln \tau} = 0 \tag{11}$$

This method of deducing ν is preferred over the method of moments because of its relative insensitivity to outliers (Oreopoulos and Davies 1998b). Substituting (10), R_{pph}, and T_{pph} into (9) yields Barker's (1996) gamma-weighted two-stream approximation (GWTSA). Expressions for collimated and diffuse sources are presented in appendix A. Throughout this study, the only PPH model used was the delta-Eddington (Joseph *et al.* 1976). As the GWTSA is used in the new 1D model, this implies that cloud layers are variable in the horizontal only. This simplification is made routinely in studies of radiative transfer for inhomogeneous clouds (e.g. Stephens 1988a; Cahalan *et al.* 1994a,b; Barker *et al.* 1996).

In practice, GWTSA quantities are computed using $\bar{\tau} = \bar{\tau}_{\mathrm{cld}} + \tau_{\mathrm{clr}}$ in which $\bar{\tau}_{\mathrm{cld}}$ and τ_{clr} are for clouds and homogeneous clear-sky (effective values of ω_0 and g are computed as in (7b) and (7c) with the addition of values for clouds). This makes the lower limit on the integral in (9) τ_{clr} instead of 0. To include this would ruin the efficiency of the analytic solutions presented in appendix A. Therefore a simple adjustment is proposed. Since the standard deviation of total optical depth (i.e. clear + cloud) equals that for cloud only, if it is assumed that (10) describes the distribution of cloud τ perfectly, then based on the method of moments in which $\nu_{\mathrm{cld}} = (\bar{\tau}_{\mathrm{cld}}/\sigma)^2$ where σ is standard deviation of cloud optical depth, ν to be used in the GWTSA equations is roughly

$$\begin{aligned} \nu &= \left(\frac{\bar{\tau}_{\mathrm{cld}} + \tau_{\mathrm{clr}}}{\sigma}\right)^2 \\ &= \nu_{\mathrm{cld}} \left(\frac{\bar{\tau}_{\mathrm{cld}} + \tau_{\mathrm{clr}}}{\bar{\tau}_{\mathrm{cld}}}\right)^2 \end{aligned} \tag{12}$$

where ν_{cld} is for clouds only and diagnosed by the LSM. Thus, for example, in spectral bands with strong gaseous absorption it may be that $\tau_{\mathrm{clr}} \gg \bar{\tau}_{\mathrm{cld}}$ and so $\nu \gg \nu_{\mathrm{cld}}$. This signifies that despite variable cloud, the overall response could be dominated by the uniform gas. Using aerosol-free standard atmospheres, it was found here (not shown) that use of (12), as opposed to ν_{cld}, had very little effect on broadband flux estimates. Barker *et al.* (1996) discussed a similar situation in which ν and $\bar{\tau}$ were based on Landsat-inferred cloud optical depths (Wielicki and Parker 1994). The non-zero lower bound on integration arose from the discretized satellite sensor. They found this to be a significant issue only for $\nu \ll 1$ and low sun (see their Fig. 3).

(c) *Overcast cloudy layers*

In general, one can expect layered clouds within LSMs to be sliced arbitrarily into multiple contiguous layers. Hence, radiation calculations must be performed on adjacent layers of horizontally variable clouds; not just on entire clouds as in previous studies (e.g. Stephens 1988b; Cahalan *et al.* 1994a; Barker 1996). This section presents an approximation for this condition for use with the multi-layer GWTSA.

Consider an overcast planar cloud that has horizontally variable τ, yet the extinction field is highly correlated in the vertical. Though irradiated uniformly from above, all other radiation fields associated with this cloud lack horizontal homogeneity. Therefore, if this cloud were sliced into several layers and if mean albedos and transmittances were computed for each cloud layer and radiative linking was achieved via (4a) and (4b), overall

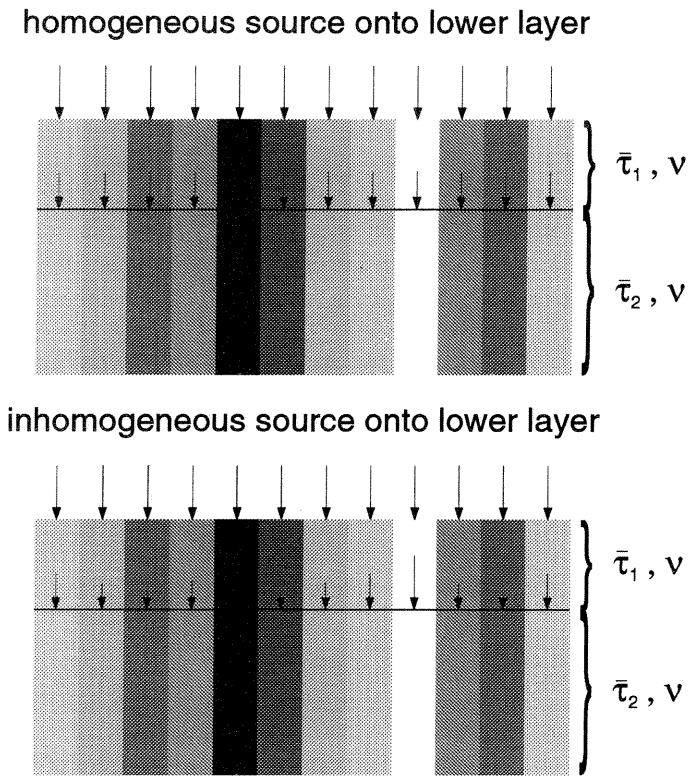

Figure 1. Single-layer cloud with horizontal variability that has been sliced into two layers with mean optical depths $\bar{\tau}_1$ and $\bar{\tau}_2$, and equal values of ν. Length of arrows denote flux (uniform onto cloudtop). Top panel shows mean transmittance through the upper layer onto the lower layer as a 1D model would predict; horizontal uniformity. Bottom panel shows that the flux onto the lower layer is variable but with a mean value equal to the corresponding value in the top panel. The perfect vertical correlation for these layers is like that for the contiguous multi-layer cascade clouds when clouds in all layers are generated with the same sequence of random numbers (see section 4(b)).

mean albedos and transmittances would be between the true values (computed for the cloud as a single layer) and corresponding PPH values. This is because (4a) and (4b) implicitly homogenize internal fluxes and for this to be enforced on horizontal variable clouds represents a discrete step towards the PPH solution. Figure 1 shows a schematic cloud sliced in two. If T_1 is the proper *mean* transmittance for the first layer but it is assumed that the top layer does *not* give rise to a variable radiation field exiting its base, too much radiation will impinge dense regions of the lower layer while too little radiation will impinge tenuous regions. Hence, the lower layer is irradiated improperly: too much weight is given to thick regions and too little to thin regions.

A parametrization for the GWTSA to utilize (4) yet deal with this correlation between radiation and extinction (cf. Stephens 1988b) is now presented. For clarity, it is illustrated for normal direct-beam transmittance, where it is exact, and then extended to diffuse fluxes, where it is approximate. Assuming that the distribution of τ for the entire cloud in Fig. 1 follows $p_\Gamma(\tau)$, domain-averaged direct-beam transmittance is

$$T_\Gamma^{\mathrm{dir}} = \int_0^\infty p_\Gamma(\tau) e^{-\tau}\, \mathrm{d}\tau = \left(\frac{\nu}{\nu + \bar{\tau}}\right)^\nu \tag{13}$$

where $\bar{\tau}$ is again transformed for forward-scattering [note that for the GWTSA this expres-

sion replaces (2)]. Subdivide the cloud into N equal layers each with mean optical depth $\bar{\tau}/N$ and ν equal to the original ν (which follows from perfect vertical correlation). In the spirit of (5), if layer mean transmittances are multiplied, domain-averaged transmittance is

$$T_{\Gamma}^{\mathrm{dir}}(N) = \prod_{n=1}^{N} \left(\frac{\nu}{\nu + \bar{\tau}/N} \right)^{\nu} = \left(\frac{\nu N}{\nu N + \bar{\tau}} \right)^{\nu N} \tag{14}$$

which can be shown by induction to be less than $T_{\Gamma}^{\mathrm{dir}}$. Moreover,

$$\lim_{\{N \text{ or } \nu\} \to \infty} \left(\frac{\nu N}{\nu N + \bar{\tau}} \right)^{\nu N} = e^{-\bar{\tau}} \tag{15}$$

shows that N going to infinity is tantamount to ν going to infinity (i.e. homogeneity) and that the standard 1D methodology fails.

Now, relax the constraint that sublayers be of equal thickness, and denote the n^{th} layer's density function as $p_{\Gamma n}(\tau)$ which is defined by ν and $\bar{\tau}_n$ ($\sum_{n=1}^{N} \bar{\tau}_n = \bar{\tau}$). Then, by virtue of perfect vertical correlation, weighting $p_{\Gamma n}(\tau)$ by incident energy and renormalizing yields

$$p_{\Gamma_n^*}(\tau) = \frac{1}{\Gamma(\nu)} \left(\frac{\nu + \sum_{k=0}^{n-1} \bar{\tau}_k}{\bar{\tau}_n} \right)^{\nu} \tau^{\nu-1} \exp\left[-\tau \left(\frac{\nu + \sum_{k=0}^{n-1} \bar{\tau}_k}{\bar{\tau}_n} \right) \right] \equiv \frac{1}{\Gamma(\nu^*)} \left(\frac{\nu^*}{\bar{\tau}_n^*} \right)^{\nu^*} \tau^{\nu^*-1} e^{-\nu^* \tau / \bar{\tau}_n^*} \tag{16}$$

which is an altered distribution for the n^{th} layer in which $\bar{\tau}_0 = 0$ implies that $p_{\Gamma_1^*}(\tau) = p_{\Gamma_1}(\tau)$ (unaltered top layer). From (16) it can be shown (see appendix B) that the new optical properties of the layers are

$$\nu^* = \nu \tag{17a}$$

and

$$\bar{\tau}_n^* = \frac{\nu \bar{\tau}_n}{\nu + \sum_{k=0}^{n-1} \bar{\tau}_k} \leqslant \bar{\tau}_n. \tag{17b}$$

Now, when direct-beam transmittances are computed for N layers using (17) and multiplied (i.e. working with horizontally homogeneous internal radiation fields), domain-averaged transmittance is

$$T_{\Gamma^*}^{\mathrm{dir}}(N) = \underbrace{\left(\frac{\nu}{\nu + \bar{\tau}_1} \right)^{\nu} \cdot \left(\frac{\nu + \bar{\tau}_1}{\nu + \bar{\tau}_1 + \bar{\tau}_2} \right)^{\nu} \cdot \ldots \cdot \left(\frac{\nu + \sum_{k=1}^{N-1} \bar{\tau}_k}{\nu + \sum_{k=1}^{N} \bar{\tau}_k} \right)^{\nu}}_{N \text{ times}} = \left(\frac{\nu}{\nu + \bar{\tau}} \right)^{\nu} \tag{18}$$

which equals $T_{\Gamma}^{\mathrm{dir}}$ in (13). In addition to this, downward reduction of $\bar{\tau}_n$ yields correct direct-beam flux profiles too. As long as independent columns are assumed, this applies to $\mu_0 < 1$ also. For real clouds, however, minor deviations for $\mu_0 < 1$ can be expected (Gabriel and Evans 1996; Barker and Wielicki 1997).

The same type of correction is proposed for use with diffuse radiation fields. Ideally, therefore, $p_{\Gamma_n}(\tau)$ should be weighted by $T_{\text{pph}}(\mu_0, \tau)$ instead of the exponential function used above. Use of the exponential function, however, has the convenient property of leaving $p_{\Gamma_n^*}(\tau)$ as a gamma distribution. Hence, the following parametrization was derived:

$$e^{-\mathcal{D}\bar{\tau}/\mu_0} \approx T_{\text{pph}}(\mu_0, \tau) \tag{19}$$

where $\mathcal{D}$ forces T_{pph} into the Beer–Bouger–Lambert law and the left side of (19) is used to generate $p_{\Gamma_n^*}(\tau)$. For a fairly wide range of τ, asymmetry parameter near 0.85, and single-scattering albedo greater than 0.9,

$$\mathcal{D}(\mu_0) = 0.063\mu_0(2 - \mu_0) \tag{20}$$

satisfies (19) well enough for our purposes (as it gets integrated over all τ in the end).* Hence, downward adjusted $\bar{\tau}_n$ are approximated as

$$\bar{\tau}_n^* = \frac{\nu_n \bar{\tau}_n}{\nu_n + \mathcal{D}(\mu_0) \sum_{k=k_{\text{top}}}^{n-1} \bar{\tau}_k/\mu_0} \tag{21}$$

where k_{top} is the cloudtop layer, which is the same as (16) except there $\mathcal{D} = 1$.

In the derivation and application of (21), it was assumed that contiguous layers above the n^{th} layer have ν equal to ν_n, despite their likely uniqueness. As shown later, this may be neither too severe nor unreasonable. Also, when applying this algorithm, (21) is used to adjust the optical depth for both direct-and diffuse-beams. This was found to have little effect on fluxes and saved on computation of a separate adjusted optical depth for direct-beam.

Note that a column will have more than one value of k_{top} when two or more blocks of contiguous cloudy layers are separated by cloudless layers. The assumption used here is that $\bar{\tau}_n$ for the top layer of *all* contiguous blocks of clouds is unaltered. This implies no correlation between incident radiation and extinction fluctuations of the uppermost layer of a block of cloudy layers (Stephens 1988b). In a domain-averaged sense, this is equivalent to saying that incident radiation is uniform; which is the case only for the extreme uppermost layer of cloud, but need not, and almost certainly never would, be true for the top layer of lower cloud blocks. This is simply an extension of the concept of randomly overlapping partly cloudy layers except it pertains to fluctuations within overcast layers.

(*d*) *Partly cloudy layers*

Following from the argument just made, when partly cloudy layers are separated by a clear layer, it is assumed again that there is no correlation between incident radiation and extinction fluctuations of the uppermost layer of a block of cloudy layers. Hence, the GWTSA solutions with unaltered $\bar{\tau}$ for the uppermost layer in a block of cloudy layers are used in (4a) and (4b), which in turn are used in (6).

As already discussed in the context of optical depth, contiguous cloudy layers can be expected to possess a fairly high degree of vertical correlation and this extends naturally to cloud fraction (Tian and Curry 1989): thus the rationale behind the standard assumption of maximal overlap of contiguous partly cloudy layers (Geleyn and Hollingsworth 1979). The simple approach taken here of reducing $\bar{\tau}_n$ assumes that clouds in layer n are maximally overlapped with clouds immediately above in layer $n - 1$ and if $C_{n-1} \leqslant C_n$,

* By no means are we implying that (19) and (20) can substitute safely for regular application of the two-stream approximation.

the excess cloud in layer n is, in essence, randomly overlapped with clouds above layer $n-1$. Therefore, following the approach used to transform $\bar{\tau}_n$ into $\bar{\tau}_n^*$ (see Eq. (21)), mean optical depths passed to the radiation model are

$$\bar{\tau}_n^{***} = \begin{cases} \dfrac{C_{n-1}\bar{\tau}_n^{**} + (C_n - C_{n-1})\bar{\tau}_n}{C_n}, & C_{n-1} \leqslant C_n \\ \bar{\tau}_n^{**}, & C_{n-1} > C_n \end{cases} \tag{22a}$$

where

$$\bar{\tau}_n^{**} = \frac{\nu_n \bar{\tau}_n}{\nu_n + \mathcal{D}(\mu_0) \sum_{k=k_{\text{top}}}^{n-1} \mathcal{A}_k \bar{\tau}_k / \mu_0} \tag{22b}$$

in which

$$\mathcal{A}_k = \begin{cases} (1 - C_k)^{-1}, & C_k \leqslant 0.5 \\ C_k^{-1}, & C_k > 0.5. \end{cases} \tag{22c}$$

For computational economy, both the overlapped and non-overlapped portions of a cloudy layer use the same $\bar{\tau}_n^{***}$ and ν_n (which stems from the assumption that both portions are statistically identical). Moreover, the empirical function $\mathcal{A}_k$ was found to improve results relative to $\mathcal{A}_k = 1$ for a wide variety of experiments. In a crude way, this mimics the effects of maximal/random cloud overlap by counteracting errors introduced by (6).

3. Model roster

This section describes briefly the models whose results are presented in the following section. All the column models used here have been implemented in two 1D broadband algorithms: one resembling very closely that used in the NCAR general circulation models (GCMs) (Briegleb 1992); and that used in the Canadian GCM (McFarlane *et al.* 1992; Barker and Li 1995). Though the algorithms used in these GCMs are quite different, the impact of the GWTSA was almost identical. Results presented in this paper are for the NCAR model which divides the solar spectrum into four bands (18 pseudo-bands) with cloud optics defined by Slingo's (1989) parametrization. See Briegleb (1992) for performance details.

The multi-layer version of the GWTSA that uses $\bar{\tau}^{***}$ is referred to hereinafter as the *corrected*-GWTSA (c-GWTSA). Since the c-GWTSA is the primary model presented in this paper, it is contrasted with three other 1D approximations. First is its counterpart that utilizes simply $\bar{\tau}$. This model is referred to as the *uncorrected*-GWTSA (uc-GWTSA). Second is the regular PPH two-stream approximation which uses R_{pph}, T_{pph}, r_{pph}, and t_{pph}. Third is Cahalan *et al.*'s (1994a) effective thickness approximation (ETA). For the ETA, layer fluxes are computed by the zero$^{\text{th}}$-order term of the PPH model's Taylor series expansion about $\overline{\ln \tau}$. The ETA uses the PPH solutions, but instead of operating on $\bar{\tau}$, it operates on $\eta\bar{\tau}$ where

$$\eta = \frac{e^{\overline{\ln \tau}}}{\bar{\tau}} \leqslant 1. \tag{23}$$

Clearly, η depends on $p(\tau)$ and for $p_\Gamma(\tau)$,

$$\eta = \frac{e^{\psi(\nu)}}{\nu} \tag{24}$$

where ν is from the MLE method (see Eq. 11).

The column models were assessed as follows. Beginning with either 2D (vertical and one horizontal direction) or 3D domains containing inhomogeneous clouds, create profiles of the necessary horizontally-averaged optical properties needed to drive the column models (i.e. layer values of C, $\bar{\tau}$, ω_0, g, ν, η, and $\bar{\tau}^{***}$). Benchmark calculations were computed, for the most part, with the ICA model (see Eq. (8)). As with single-layers, multi-layer ICA results are obtained by applying a regular 1D-PPH model to each column in a domain and then averaging fluxes horizontally. In the ICA, cells in each column are either full or free of cloud. Layer reflectances and transmittances (clear and cloudy portions) for *all* models mentioned so far are based on the delta-Eddington approximation (Joseph *et al.* 1976). Also, layer fluxes are linked according to Eqs. (1) through (6).

When cloud-resolving model (CRM) data were used, geometric sizes of grid-cells were defined thus enabling straightforward application of a Monte Carlo (MC) photon transport algorithm (Barker *et al.* 1998). This provides an indication of the importance of neglecting finite cloud effects. As in the column models, scattering and absorption occur in the MC simulations at scattering events. Effective single-scattering properties are exactly those in the column models though the Henyey–Greenstein (1941) scattering phase function is used. The number of photons injected per band is proportional to incident flux density at the TOA. Hence, absorption and spectral integration are treated identically in all models. Underlying surfaces are Lambertian, and cyclic horizontal boundary conditions are used. For multi-layered atmospheres containing overcast PPH clouds, the MC and the column model agree typically to within ~1% for boundary fluxes and ~3% for heating rates. The exception being very oblique sun where the delta-Eddington is known to be deficient (King and Harshvardhan 1986). Also, results presented are integrations over solar azimuth angle.

4. Results and discussion

This section consists of three main subsections. First, the single-layer GWTSA is assessed using idealized $p(\tau)$ from a phenomenological fractal generator. Second, results for the multi-layer c-GWTSA are compared with results for the other column models using, again, model fractal clouds. Third, data from CRMs are used to conduct more definitive tests of the multi-layer c-GWTSA.

(a) *Single-layer bounded cascade clouds*

To give an idea of the capabilities of the GWTSA, fluxes were computed for single-layer cloud-forms generated by Cahalan *et al.*'s (1994a) 1D bounded cascade model. This method of generating horizontally inhomogeneous clouds was used because of its simplicity and because its (discrete) density functions of τ *are not* gamma distributions. Actually, liquid water paths $\mathcal{L}$ (g m^{-2}) were simulated and optical depths for four spectral intervals were computed as

$$\tau_j = \mathcal{L}\left(a_j + \frac{b_j}{r_e}\right); \quad j = 1, \ldots, 4 \tag{25}$$

where a and b are coefficients (Slingo 1989), and r_e is effective radius of cloud droplets. Spectral values of ω_0 and g were also computed with Slingo's four-band parametrization. As long as r_e is constant across a cloud field, and this was the case throughout this study with $r_e = 10$ μm unless stated otherwise, histograms for $\mathcal{L}$ and τ have the same ν (which does not vary spectrally). Two parameters govern clouds produced by this model: $0 \leqslant f \leqslant 1$ which controls var($\mathcal{L}$); and $0 \leqslant c \leqslant 2$ which controls autocorrelation in $\mathcal{L}$. All results

presented here used $c = 0.794$ which yields fields whose power spectra have slopes near -1.5 when plotted on log-log scales. This model was extended to generate partly cloudy conditions (Barker and Davies 1992; Marshak *et al.* 1998). Appendix C gives a brief description of the bounded cascade model, assesses its behaviour for partly cloudy cases, and compares it to results from Landsat imagery.

Figure 2 shows PPH, ETA, GWTSA, and ICA albedos and absorptances for a range of overcast conditions. These are broadband values for droplets only. For small f, cloud variability is sufficiently weak that all models, including the PPH compare well with the ICA. When $\bar{\tau}/\mu_0$ is small ($\lesssim 10$), the ETA increasingly under-reflects and under-absorbs as f increases. This is due to neglect of the second-order term in the Taylor expansion of $R_{\text{pph}}(\overline{\ln \tau})$ which is positive and increases monotonically with f. As $\bar{\tau}/\mu_0$ becomes larger, this term eventually becomes negative and is responsible for the slight overestimation at small f for $\bar{\mathscr{L}}$ of 120 g m^{-2}. The GWTSA has a clear tendency to overestimate albedo and absorptance relative to the ICA. For the most part, however, its curves are closer to the ICA curve than are the ETA curves. As can be seen in appendix C, truncated cascade fields with $C < 1$ are described by $p_\Gamma(\tau)$ much better than untruncated fields. Thus, for $C < 1$, the GWTSA will perform much better than as shown in Fig. 2.

(*b*) *Multi-layer atmospheres with bounded cascade clouds*

The parametrizations presented in section 2(a) are now demonstrated with bounded cascade clouds. Throughout this subsection, clouds that are in contiguous layers were created with the same random number sequence, which produces perfect vertical correlation (see Fig. 1), whereas non-contiguous clouds were created with different random sequences.

As discussed above, a cloud's albedo should be independent of the number of layers it is sliced into. Figure 3 shows contours of GWTSA albedo differences, weighted by μ_0, between single-layer cloud albedos and albedos computed for the same clouds after they have been sliced in two. These are for overcast cascade clouds generated with $f = 0.5$ and no atmosphere aside from cloud droplets. The column of plots labelled *uncorrected* correspond to differences when two-layer albedos were computed without downward adjustment of τ (i.e. the uc-GWTSA model). The column of plots labelled *corrected* is for downward reduced τ according to (22) (i.e. the c-GWTSA model). When the fraction of the cloud in the upper layer is either 0 or 1, differences are zero as these limiting cases are single layers. The *uncorrected* plots have the largest errors and are almost symmetric about slicing the cloud in half. These overestimates of albedo by the two-layer system arise because the thick portions of the lower clouds have effectively received too much irradiance and thus reflect too much radiation. The panels for the c-GWTSA show that when $\bar{\tau}$ of the lower layer is reduced according to (22), errors associated with two-layer systems are generally two to ten times smaller than for the uc-GWTSA.

Figure 4 demonstrates further the impact of adjusting $\bar{\tau}$ for the lower layer as it shows overall GWTSA albedos for the same cloud used in Fig. 3 ($\bar{\mathscr{L}} = 120$ g m^{-2}) as a function of number of equal layers into which the cloud is partitioned (ranging from 1 single layer to 30 layers each having $\bar{\mathscr{L}} = 4$ g m^{-2}). Just as for direct-beam (see Eqs. (14) and (15)), as the number of layers increases, uc-GWTSA albedo approaches the PPH value. When the correction is applied, however, albedo is much less sensitive to the number of layers. Perfect insensitivity was not expected since $\bar{\tau}$ were adjusted based on the primary stream of radiation only; not for multiply reflected internal beams. This explains in part the sudden dip in going from one to two layers: the upper half of the cloud, with unadjusted $\bar{\tau}$, is not transmissive enough to radiation reflected by the lower layer.

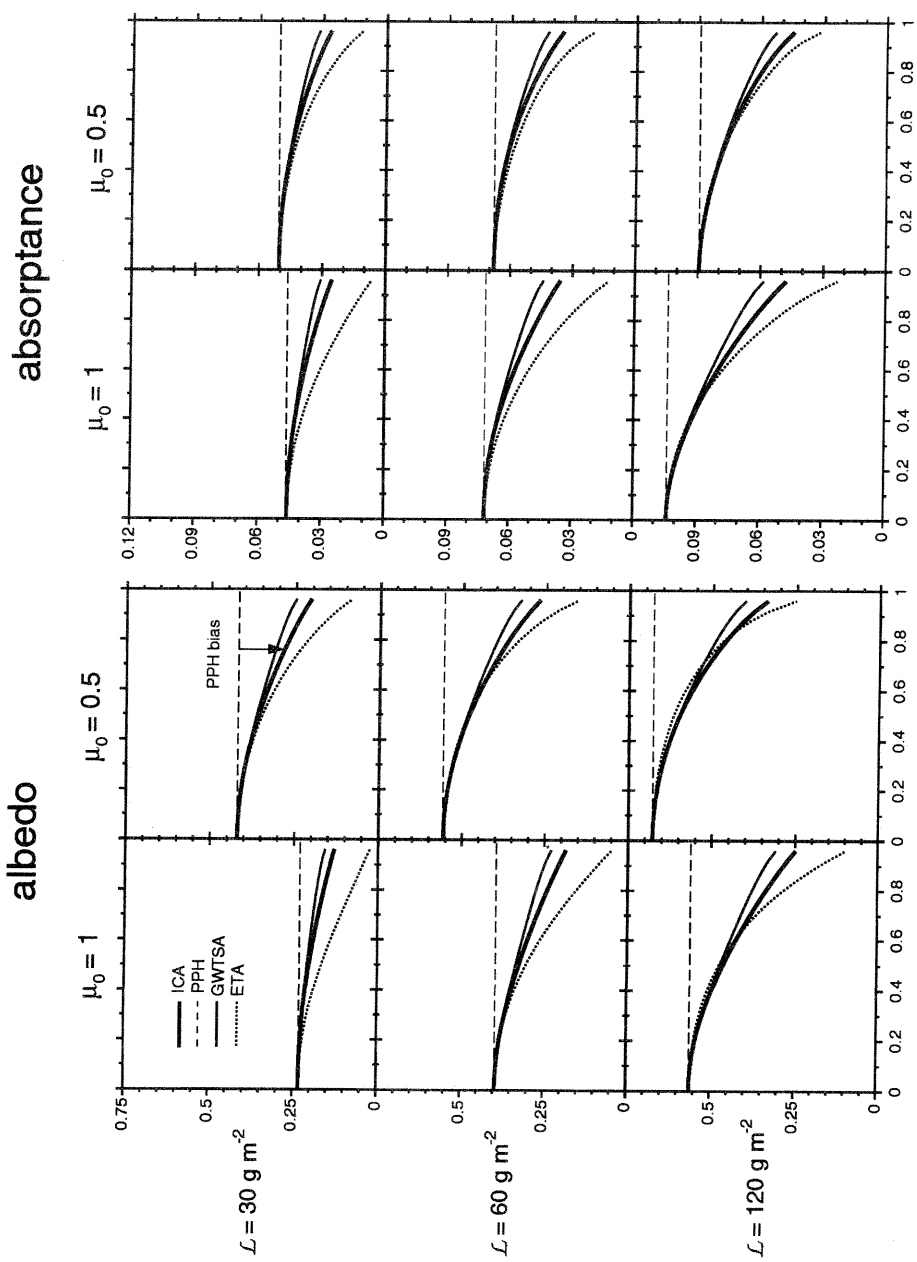

Figure 2. Broadband albedos and absorptances for overcast, single-layer bounded cascade clouds as a function of f (the parameter that controls the variance of τ; see appendix C). Attenuation is by cloud droplets only. Results are shown for two values of cosine of solar zenith angle μ_0 and three values of mean cloud liquid water path $\mathscr{L}$. Independent column approximation (ICA) values represent the standard; plane-parallel, homogeneous (PPH); effective thickness approximation (ETA); and GWTSA using ν generated by the MLE method are also shown.

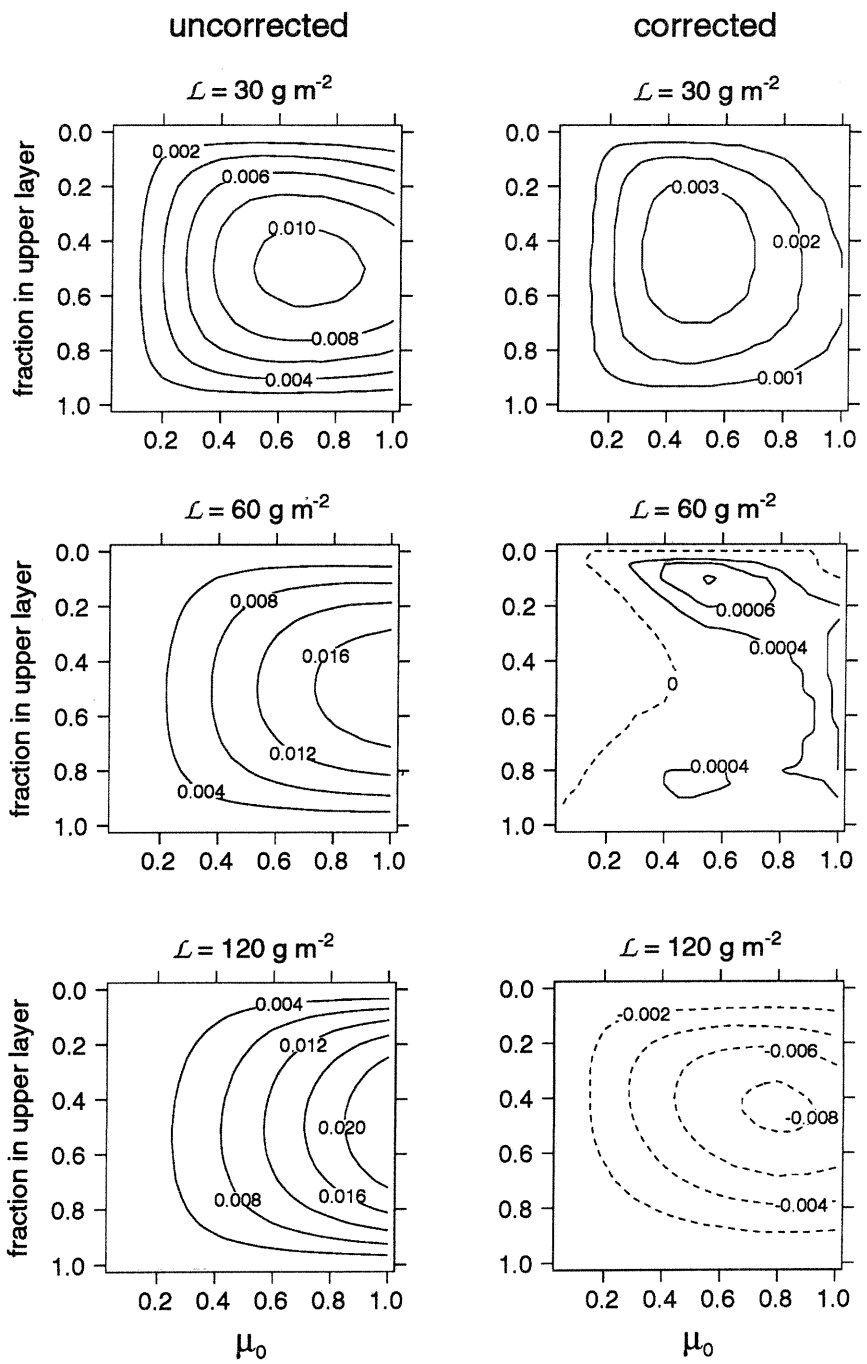

Figure 3. Contours are differences, multiplied by μ_0, between broadband albedos (cloud droplets only) for overcast, single-layer bounded cascade clouds ($f = 0.5$) and the same clouds when they are partitioned into two layers (see Fig. 1). Differences are zero when the fraction of cloud in the upper layer is either 0 or 1. Results are shown as a function of μ_0 for three values of mean liquid water path $\mathcal{L}$. Column labelled *uncorrected* is for the GWTSA when the mean optical depth $\bar{\tau}$ of the lower layer is unadjusted. Column labelled *corrected* is when $\bar{\tau}$ of the lower layer is reduced according to Eq. (22).

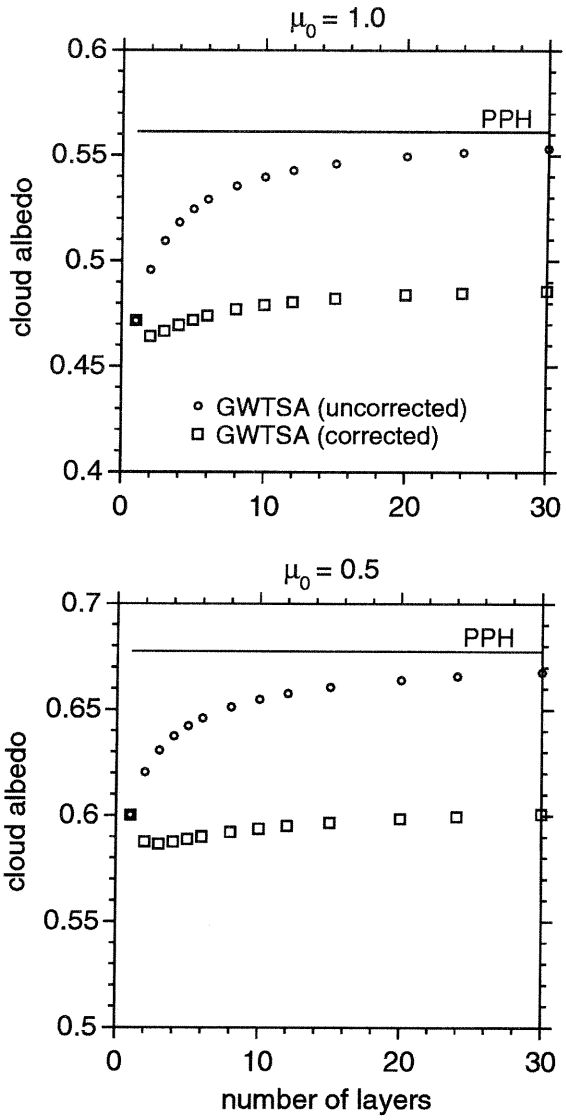

Figure 4. Broadband albedos for overcast, bounded cascade clouds ($f = 0.5$) with $\mathcal{L} = 120$ g m^{-2} as functions of number of equal layers into which the cloud was partitioned. Circles represent values for the GWTSA when mean layer optical depths $\bar{\tau}$ are unadjusted. Squares are the same but $\bar{\tau}$ were reduced according to Eq. (22). The PPH value, which is independent of number of layers, is shown for reference.

Like the PPH model, ETA albedos and transmittances are independent of the number of layers a cloud is broken into. This may seem odd given that the ETA does not apply to thin layers (see Cahalan *et al.* 1994a; and Fig. 2 of this paper). By effectively irradiating internal layers incorrectly (i.e. homogeneously), this counteracts the ETA's inappropriateness for each layer and rescues it (when it applies) with respect to diffuse fluxes. Problems can, however, be expected to arise with heating rate profiles. Also, when higher-order Taylor expansion terms are retained (Cahalan *et al.* 1994a; Barker 1996), the ETA's lack of dependence on number of layers vanishes.

TABLE 1. CLOUD CHARACTERISTICS FOR THE EXPERIMENTS WITH MULTI-LAYERED BOUNDED CASCADE CLOUDS.

	case 1			case 2			case 3		
σ	C	$\bar{\mathcal{L}}$	ν	C	$\bar{\mathcal{L}}$	ν	C	$\bar{\mathcal{L}}$	ν
0.50	0	—	—	0	—	—	0	—	—
0.55	0	—	—	0	—	—	0	—	—
0.60	0	—	—	0	—	—	1.0	27	1.50
0.65	0	—	—	0	—	—	1.0	27	1.50
0.70	0	—	—	0	—	—	0	—	—
0.75	0	—	—	0	—	—	0	—	—
0.79	0	—	—	0	—	—	1.0	35	1.50
0.83	0	—	—	0.3	35	1.10	1.0	35	1.50
0.87	1.0	55	1.50	0.5	42	1.12	0	—	—
0.90	1.0	40	1.50	0.7	30	1.17	0	—	—
0.93	1.0	40	1.50	0.5	30	1.12	1.0	30	1.50
0.95	1.0	25	1.50	0.3	16	1.10	1.0	30	1.50
0.97	0	—	—	0	—	—	0	—	—
0.99	0	—	—	0	—	—	0	—	—
1.0	0	—	—	0	—	—	0	—	—

C and $\bar{\mathcal{L}}$ denote layer cloud fraction and mean liquid water path (g m^{-2}) and ν is defined by (11). σ is p/p_{srf} where p is pressure at the base of a layer and p_{srf} is surface pressure. The 15 layers above those listed here were devoid of clouds. Gaseous and temperature profiles followed the midlatitude summer standard; surface albedo was 0.1 across the spectrum.

The following experiments included fractal clouds imbedded in midlatitude summer profiles of temperature and gas concentrations (McClatchey *et al.* 1972). Table 1 lists cloud and other boundary conditions used for these experiments. Figure 5 shows TOA albedo α_p, atmospheric transmittance T_p, and heating rate (HR) differences between the ICA and four models: PPH, ETA, uc-GWTSA and c-GWTSA for the cases listed in Table 1. Case 1 is similar to clouds used so far: a single overcast cloud split into four layers. Both the ETA and c-GWTSA have closed the PPH-biases for α_p and T_p by more than 75% typically. HR differences show that the ETA has pronounced under- and over-absorption in the uppermost layer and in lower layers, respectively. In fact, its error tracks that of the uc-GWTSA, primarily because both lack an adjustment to lower layer $\bar{\tau}$. The c-GWTSA, however, under-absorbs only slightly throughout most of the cloud. The PPH model exhibits anomalous heating near cloudtop and much reduced heating below (cf., Barker *et al.* 1998).

Case 2 has a vertically-projected cloud fraction of 0.7 and maximal overlap is assumed. Typically, PPH-biases are about ± 0.1 for α_p and T_p which correspond to relative errors of roughly 30%. The biases have increased relative to the previous case because the truncated cascade fields yield smaller ν (see Table 1 and appendix C). The uc-GWTSA has closed these biases by only $\sim$25%. Just as in case 1, HR errors for the PPH model show excessive heating in the upper reaches of the clouds and weak heating near cloudbase and beneath cloud. The uc-GWTSA's HR errors track PPH errors closely but are shifted towards cloudbase, due to larger transmittances, with little error near cloudtop.

While the ETA has almost closed the PPH-biased at high sun, at mid to low sun it does only marginally better than the uc-GWTSA. This is because for the cloud on the whole, the ETA is beyond its ideal range; i.e. neglect of higher-order terms (which are negative because $\bar{\tau}/\mu_0$ is large) make the ETA overestimate albedo. The c-GWTSA, on the other

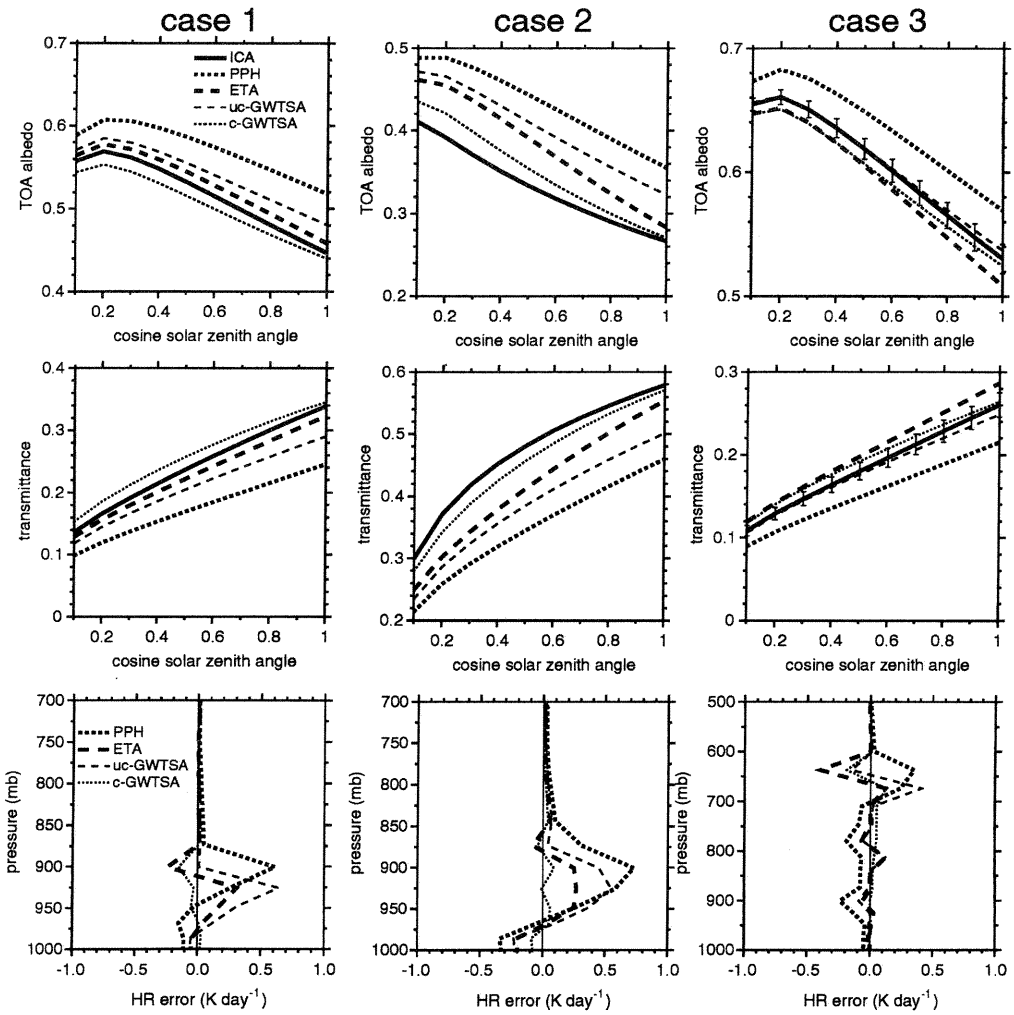

Figure 5. Broadband TOA albedo and atmospheric transmittance as a function of μ_0 for the three cases of bounded cascade clouds documented in Table 1. Results are for five models as indicated on the plot. For case 3, the ICA model has error bars on albedo and transmittance. These indicate the standard deviation for ten realizations. Also shown are heating rate differences between the listed models and the ICA model which was assumed to be the standard.

hand, closed the PPH-biases by more than 85% for most μ_0. Moreover, the c-GWTSA's HR errors are typically three times smaller than those for other models.

Case 3 has three non-contiguous groups of overcast clouds, each consisting of two overcast layers. Therefore, this experiment tests the c-GWTSA hypothesis that $\bar{\tau}$ for the top layer of the middle and lower blocks of clouds should not be adjusted (the lower layer for these cloud blocks, however, are adjusted). In order to realize better the notion that non-contiguous clouds have randomly overlapping fluctuations, ICA quantities presented here are ensemble-averages for 10 simulations each of which used unique sequences of random numbers to generate the cascade clouds. As expected, Fig. 5 shows that, because of the randomization of τ, PPH-biases for α_p and T_p are small compared to the contiguous cloud cases. Had all the clouds been generated by the same random sequence, PPH-biases

would have been comparable to those in the previous cases because ICA values of α_p and T_p would have been respectively smaller and larger than those shown in Fig. 5 (PPH, ETA, and uc-GWTS values are insensitive to these correlations). The ETA slightly over-corrects the PPH-biases as does the c-GWTSA for low sun, though for high sun the c-GWTSA performs well. The uc-GWTSA performs almost perfectly (i.e. well within the standard deviation of ICA values), but its HR errors are significantly larger than those for the c-GWTSA. Again, the PPH displays excessive heating in the upper cloud, and too little heating below due to too little transmittance through the upper cloud.

These experiments were also run using surface albedo of 0.8. With respect to boundary fluxes, the c-GWTSA performed slightly worse than as shown in Fig. 5 but the PPH-biases were small. When surface albedos are this large, however, μ_0 is usually small (i.e. high latitudes). Thus, transmittances are reduced which mitigate the importance of adjustments to $\bar{\tau}$. Also, in cold climates, clouds may resemble PPH conditions well, thus ameliorating the need to invoke the GWTSA. As for heating rates, profiles for the c-GWTSA were still the most superior by far.

(c) *Cloud-resolving model (CRM) atmospheres*

Thus, far, the c-GWTSA has been applied to idealized atmospheres. The ultimate intention is that it work well for *real* atmospheres (which can be assumed to exist at scales unresolved by LSMs). At this stage, the best descriptions of realistic, multi-dimensional cloudy atmospheres come from CRMs with horizontal grid-spacings preferably less than 2 km. Therefore, the c-GWTSA is now assessed using atmospheres generated by 2D and 3D CRMs. In all cases, surface albedo is 0.1 across the entire solar spectrum.

The 2D field is from Fu *et al.*'s (1995) simulation of a tropical convective system. Horizontal grid-spacing is 1 km and domain size is 512 km. There are 34 layers of variable thickness. In addition to standard profiles for ozone and the uniformly mixed gases, only model-generated water vapour and cloud liquid water were used; graupel, snow, rain, and ice were neglected because of ambiguities setting single-scattering properties and determining ν. Figure 6 shows total $\mathscr{L}$ as a function of distance. Clearly this field is very inhomogeneous as ν for $\mathscr{L}$ is just 0.48. Figures 7(a) and 7(b) show layer values of C, ν, and $\bar{\tau}$. These profiles are the only information passed to 1D models. While most layers have C near 0.12, vertically-projected cloud fraction is 0.5. This indicates that clouds in contiguous layers are neither maximally nor randomly overlapped. Most layers have $\nu \approx 1$ which is small but still much larger than that for total τ (i.e. 0.48) Figure 7(b) shows layer values of total $\bar{\tau}$ (all constituents) and $\bar{\tau}^{***}$ as used by the c-GWTSA at $\mu_0 = 0.5$. For almost all layers $\bar{\tau}^{***} \ll \bar{\tau}$. If the curve for $\bar{\tau}$ is multiplied by $\sim$0.57, one obtains the approximate optical depth profile that would be used by the ETA.

Figures 8(a) and 8(b) show domain-averaged α_p and T_p for the 2D field. Agreement between the MC and ICA for $\mu_0 \geqslant 0.5$ is almost perfect. For smaller μ_0, the MC reflects more and transmits less than the ICA. This is because the MC experiences direct irradiance onto cloud sides (Welch and Wielicki 1984) and the ICA uses the delta-Eddington (King and Harshvardhan 1986). The c-GWTSA performs almost as well as the ICA, whereas the PPH model performs terribly committing albedo and transmittance errors that are typically about $\pm 60\%$.

Domain-averaged HR profiles for the 2D field are shown in Figs. 8(c) and 8(d). As expected, the ICA and MC profiles are in excellent agreement throughout the entire atmosphere. The c-GWTSA underestimates slightly near 600 mb. This is most likely due to an over-reduction in optical depth. Otherwise, at $\mu_0 = 1$, agreement with the ICA is excellent while for $\mu_0 = 0.5$, it is equally good above most of the clouds but underestimates below 700 mb. As with the cascade clouds and in Barker *et al.* (1998), the PPH HR profile

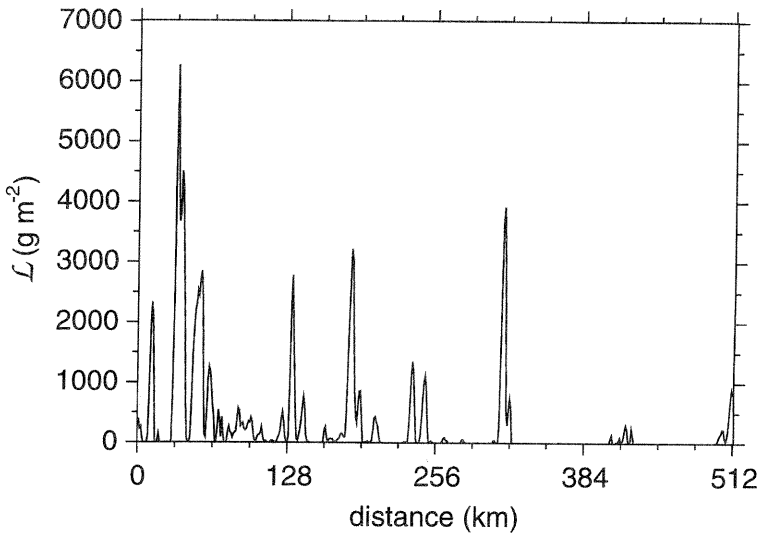

Figure 6. Liquid water path $\mathcal{L}$ for the domain of a 2D cloud-resolving model simulation (Fu *et al.* 1995).

is characterized by anomalously large heating near cloudtops and too little heating beneath. This is because in the PPH model, moderately thick clouds are spread over the entire cloudy portion of a layer and not confined, as in the 3D and ICA cases, to convective cores where they would be shielded greatly from radiation.

The 3D cloud field was generated by the Regional Atmospheric Modeling System's (Pielke *et al.* 1992) simulation of the mesoscale convective system EMEX9 (Alexander 1995). Horizontal grid-spacing is 1.5 km and domain size is 120 × 144 km. There are 34 layers of variable thickness. Again, only cloud water and vapour were used along with standard profiles of ozone and the uniformly mixed gases. Figure 9 shows the horizontal distribution of total $\mathcal{L}$ whose mean value is ~800 g m^{-2} (visible $\bar{\tau} \approx 80$). In this case, r_e was set to 15 μm. Figure 7(c) shows that most clouds were at altitudes between 800 mb and 500 mb and that $C \leqslant 0.26$ for all layers. But, since clouds in adjacent layers overlap by typically ~75%, total vertically-projected C is ~0.45. Similar to the 2D field, layer values of ν are typically near 1.0 but ν for overall τ is just ~ 0.4. Figure 7(d) shows layer values of total $\bar{\tau}$ (all constituents) and $\bar{\tau}^{***}$. Above ~600 mb, $\bar{\tau}^{***}$ are greater than about $\bar{\tau}/2$. Below ~600 mb, the parametrization in section 2 has virtually eliminated the lower third of the cloud field!

Figure 10 shows that EMEX9's PPH-biases for albedo are typically 0.15. On the other hand relative to the ICA, the c-GWTSA performs extremely well for all μ_0 closing PPH-biases by more than 90% in general. Differences between the MC and ICA are virtually identical to those shown by Barker *et al.* (1998). Note that in this case, the rapid increase in MC albedo for $\mu_0 \leqslant 0.5$ is not tracked by either the ICA or the c-GWTSA.

Figures 10(c) and 10(d) show HR profiles for the various models. As expected (see Barker *et al.* 1998), profiles for the MC and ICA agree very well. The fact that the c-GWTSA profiles follow those of the MC almost as well as the ICA justifies the huge differences between $\bar{\tau}$ and $\bar{\tau}^{***}$ shown in Fig. 7(d). At and below cloud levels, heating anomalies for the c-GWTSA are generally four to eight times smaller than those for the PPH and ETA (not shown).

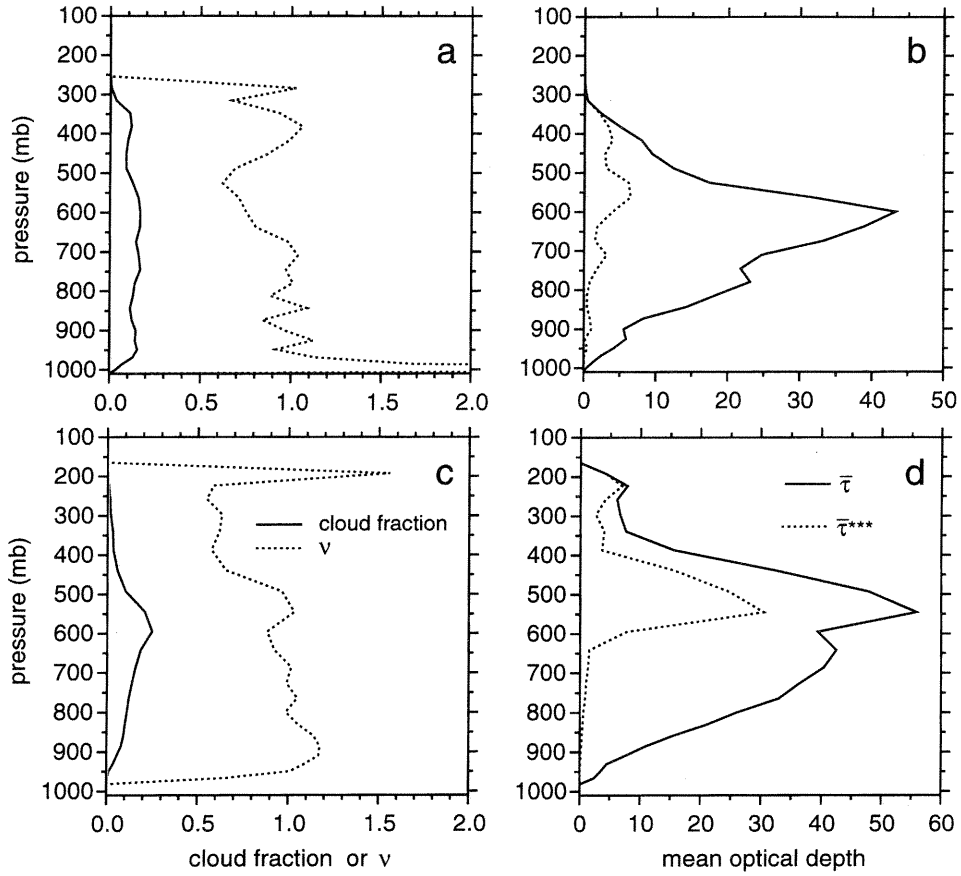

Figure 7. (a) Profiles of layer cloud fraction and ν (by the MLE method) for the 2D cloud field whose liquid water path is shown in Fig. 6. (b) Solid line represents layer mean (visible) optical depth for the 2D field as used by the PPH and uncorrected GWTSA (uc-GWTSA) models. Dashed line represents reduced optical depths (according to Eq. (22) using $\mu_0 = 0.5$) as used by the corrected GWTSA (c-GWTSA). (c) and (d) are the same as (a) and (b) but they are for a 3D cloud field (see Fig. 9).

5. Summary and Conclusion

This paper presented a new 1D solar radiative transfer model for use in LSMs such as GCMs and NWP models. The code differs from standard multi-layer column models in two ways. First, it addresses subgrid-scale cloud variability by assuming that within each grid-cell, frequency distributions for cloud optical depth τ are described well by gamma density functions $p_\Gamma(\tau)$ (Barker *et al.* 1996; Oreopoulos 1996). While regular column models use PPH two-stream approximations to compute layer albedos and transmittances, the new model computes them with analytic solutions to the integral over all τ of the PPH two-stream functions weighted by $p_\Gamma(\tau)$ (Barker 1996). Hence, the new model was referred to as the gamma-weighted two-stream approximation (GWTSA). In order to operate this model, one needs estimates of not only mean optical depth $\bar{\tau}$, as required by PPH models, but some indication of cloud variability. The second difference is an attempt to counteract the implicit 1D condition that fluxes at internal levels are homogeneous. This is done by reducing $\bar{\tau}$ for layers beneath cloudtop by amounts that depend on cloud variability and

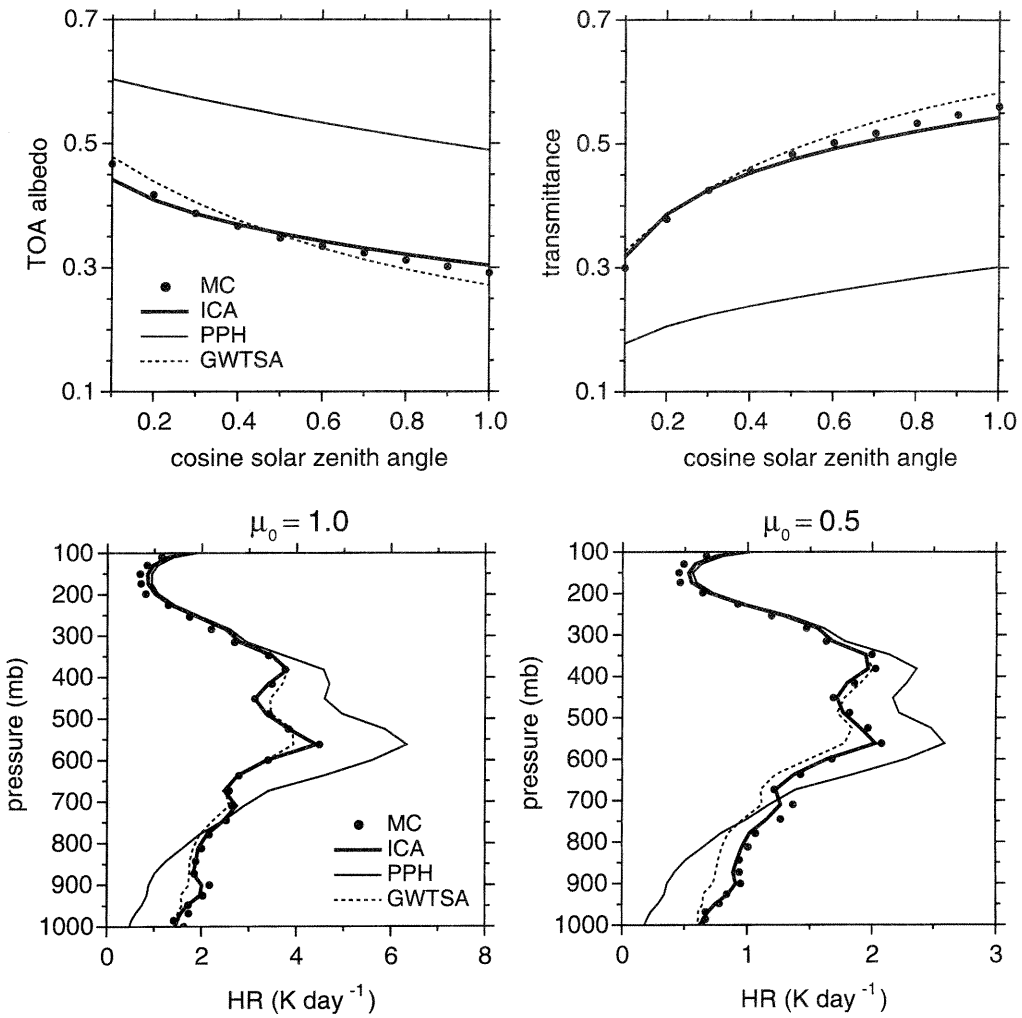

Figure 8. Broadband TOA albedo and atmospheric transmittance as a function of μ_0 for the 2D cloud field documented in Figs. 6, 7(a), and 7(b). Results are for a Monte Carlo algorithm (MC); the ICA; the 1D-PPH model; and the c-GWTSA (i.e. using $\bar{\tau}^{***}$ similar to that shown in Fig. 7(b)). Also shown are heating rate profiles for the four models at $\mu_0 = 1.0$ and 0.5.

cloud amount aloft. Moreover, investigations using CRM data are underway to incorporate a better treatment of overlapping cloud (e.g. Ritter and Geleyn 1992).

This algorithm has been implemented in two well known 1D codes; results were presented for a code that resembles very closely those used in the NCAR GCMs (Briegleb 1992). Assuming that on average, about 25% of all atmospheric cells in a 30 layer LSM contain some cloud, the vectorized multi-layer GWTSA will likely require about twice as much CPU time as its PPH counterpart. Given the magnitude of the PPH-biases often corrected by the GWTSA, doubling the CPU time devoted to solar radiative transfer seems justified.

The GWTSA was tested using 2D and 3D inhomogeneous clouds generated by a bounded cascade model and by CRMs. It operated on profiles of layer cloud fraction, $\bar{\tau}$,

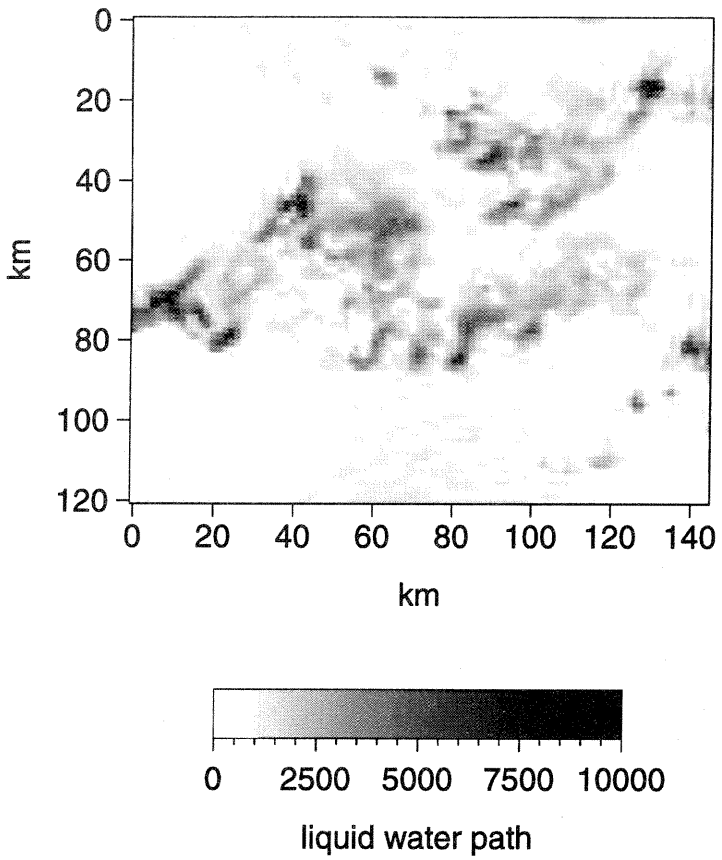

Figure 9. Liquid water path $\mathcal{L}$ for the domain of a 3D cloud-resolving model simulation (Alexander 1995).

and ν [a variance-related parameter that defines $p_\Gamma(\tau)$]. Boundary fluxes and heating rate profiles predicted by the GWTSA were compared to benchmark values determined by the ICA and a 3D Monte Carlo photon transport algorithm. It was shown that the GWTSA reduces PPH flux biases by typically more than 85% and predicts heating rates that are almost always within ± 0.1 K day^{-1} of the benchmark values.

As in Barker *et al.* (1998), these results suggest that the effects of 3D cloud geometry are of secondary importance for fluxes averaged over grids the size of those used in conventional LSMs. Rather, it is of primary importance to convey to 1D codes information about both horizontal variability of τ in each layer and the nature of cloud overlap. Evidently, the combined effects of assuming a gamma distribution for τ and reductions to $\bar{\tau}$ by the method proposed here (which loosely considers cloud overlap effects) capture much of the required information needed to obtain satisfactory flux profiles.

The main deterrent to using the GWTSA, or any similar parametrization, in a LSM is estimation of subgrid-scale variability of τ; ν in this case. It may be helpful for post-simulation diagnostic purposes that global distributions of the effective vertical integral of ν are being developed from International Satellite Cloud Climatology Project (ISCCP) satellite data (personal communication, B. Cairns 1997) and AVHRR data (Oreopoulos and Davies 1998b), however, this knowledge is of little value in the midst of an LSM

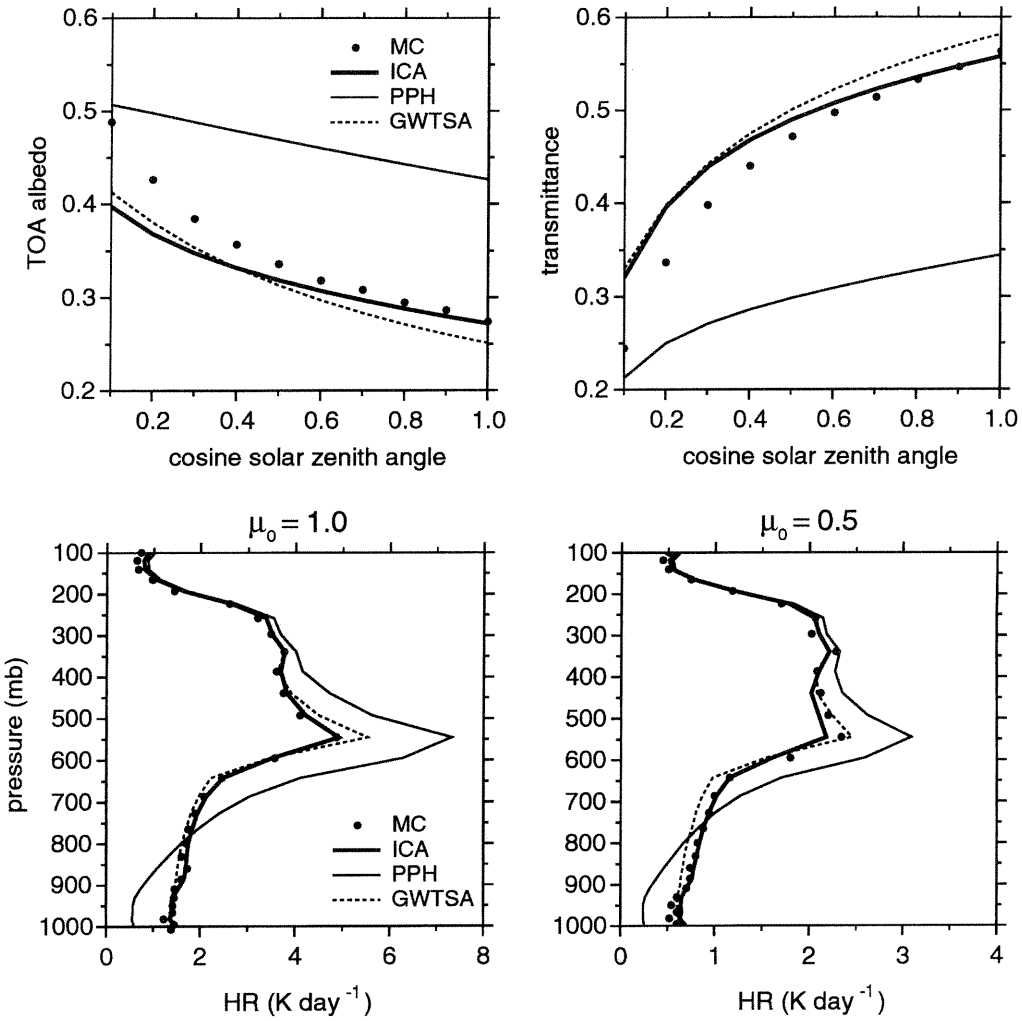

Figure 10. As in Fig. 8 except these are for the 3D field documented in Figs. 7(c), 7(d), and 9.

simulation. Evidence was presented here suggesting that for grid-spacings of $(\sim 100\ \mathrm{km})^2$, a reasonable first-order estimate of the impact on global climate due to unresolved cloud fluctuations may be achieved by making layer values of ν a diagnostic function of cloud fraction C only. A credible description, for typical LSM horizontal and vertical grid-spacings, may be as simple as: $\nu \approx 4$ for $C = 1$; decreasing to ~ 1 by $C \approx 0.9$; and holding at ~ 1 for $C < 0.9$ (see Fig. 7 and appendix C). On the other hand, if for radiative transfer purposes the atmosphere is reduced to only a few vertical layers as in Stubenrauch *et al.* (1997), these values of ν would have to be smaller in general.

The next steps beyond this study are: (i) to test the sensitivity of an LSM to inclusion of the multi-layer version of the GWTSA; (ii) develop parametrizations that convey more information about unresolved cloud fluctuations and cloud overlap; (iii) test the new algorithm with observational data; and (iv) extend the GWTSA approach to 1D infrared radiative transfer models (Barker and Wielicki 1997). Fulfillment of the last step would

enable a consistent treatment of feedbacks between subgrid-scale cloud variability, the hydrologic cycle, and both solar and terrestrial radiation.

Acknowledgements

We are very grateful to P. M. Gabriel (Colorado State U.), K. P. Shine (Assoc. Editor), and the anonymous reviewers for several constructive comments. Also, we thank Q. Fu (Dalhousie U.) and G. D. Alexander (NASA-GSFC) for providing 2D and 3D cloud-resolving model data, and R. Schemenauer (AES-ARMP) and J. D. Steenbergen (AES-ARMA) for financial support.

Appendix A

The gamma-weighted two-stream approximation (GWTSA)

The essence of the GWTSA is the assumption that probability density functions for cloud τ can often be approximated by the normalized gamma distribution $p_\Gamma(\tau)$ (see Eq. (10)). Barker (1996) showed that when the standard, non-conservative scattering two-stream approximation equations for collimated irradiance (Meador and Weaver 1980) are weighted by (10) and then integrated over all τ (see Eq. (9)), GWTSA transmittance albedo are defined as

$$T_\Gamma = \left(\frac{\nu}{\nu + \bar{\tau}/\mu_0}\right)^\nu - \phi_1^\nu \frac{\omega_0}{a}[t_+\mathcal{F}(\beta, \nu, \phi_4) - t_-\mathcal{F}(\beta, \nu, \phi_5) - t\mathcal{F}(\beta, \nu, \phi_6)] \quad \text{(A.1a)}$$

and

$$R_\Gamma = \phi_1^\nu \frac{\omega_0}{a}[r_+\mathcal{F}(\beta, \nu, \phi_1) - r_-\mathcal{F}(\beta, \nu, \phi_2) - r\mathcal{F}(\beta, \nu, \phi_3)] \quad \text{(A.1b)}$$

where

$$\mathcal{F}(\beta, \nu, \phi) = \sum_{n=0}^{\infty} \frac{\beta^n}{(\phi + n)^\nu}; \quad [|\beta| \leq 1, \beta \neq 1, \nu > 0] \quad \text{(A.2a)}$$

$$\begin{aligned} \phi_1 &= \frac{\nu}{2k\bar{\tau}}; & \phi_4 &= \phi_1 + \frac{1}{2k\mu_0} \\ \phi_2 &= \phi_1 + 1; & \phi_5 &= \phi_4 + 1 \\ \phi_3 &= \phi_4 + \tfrac{1}{2}; & \phi_6 &= \phi_1 + \tfrac{1}{2} \end{aligned} \quad \text{(A.2b)}$$

and

$$r_\pm = (1 \mp k\mu_0)(\gamma_1\gamma_3 - \gamma_2\gamma_4 \pm k\gamma_3); \quad r = 2k[\gamma_3 - (\gamma_1\gamma_3 - \gamma_2\gamma_4)\mu_0] \quad \text{(A.2c)}$$

$$t_\pm = (1 \pm k\mu_0)(\gamma_1\gamma_4 - \gamma_2\gamma_3 \pm k\gamma_4); \quad t = 2k[\gamma_4 - (\gamma_1\gamma_4 - \gamma_2\gamma_3)\mu_0] \quad \text{(A.2d)}$$

$$a = [1 - (k\mu_0)^2](k + \gamma_1); \quad k = \sqrt{\gamma_1^2 - \gamma_2^2}; \quad \beta = -\frac{k - \gamma_1}{k + \gamma_1} \quad \text{(A.2e)}$$

in which ω_0 is single-scattering albedo. The coefficients $\gamma_1, \ldots, \gamma_4$ depend on the choice of two-stream approximation, droplet single-scattering parameters, and cosine of solar

zenith angle μ_0. For the delta-Eddington solution, as used throughout this study,

$$\left.\begin{aligned} k &= \tfrac{1}{2}\sqrt{3(1-\omega_0')(1-\omega_0' g')} \\ \gamma_1 &= \frac{7-\omega_0'(4+3g')}{4} \\ \gamma_2 &= -\frac{1-\omega_0'(4-3g')}{4} \\ \gamma_3 &= \frac{2-3\mu_0 g'}{4} \\ \gamma_4 &= 1-\gamma_3 \end{aligned}\right\} \tag{A.3}$$

where ω_0' and g' are scaled values of ω_0 and asymmetry parameter. When the source is an isotropic diffuse-beam, corresponding GWTSA transmittance and albedo are

$$t_\Gamma = \phi_1^\nu \frac{2k}{(k+\gamma_1)} \mathcal{F}(\beta, \nu, \phi_6) \tag{A.4a}$$

and

$$r_\Gamma = \phi_1^\nu \frac{\gamma_2}{(k+\gamma_1)} [\mathcal{F}(\beta, \nu, \phi_1) - \mathcal{F}(\beta, \nu, \phi_2)]. \tag{A.4b}$$

In addition, Barker (1996) showed that GWTSA transmittance and albedo for a conservative scattering layer irradiated by a collimated source are

$$\begin{aligned} T_\Gamma &= \left(\frac{\nu}{\gamma_1\bar{\tau}}\right)^\nu \left[(\gamma_1\mu_0+\gamma_4)\mathcal{G}\left(1-\nu, \frac{\nu}{\gamma_1\bar{\tau}}\right) - (\gamma_1\mu_0-\gamma_3)\mathcal{G}\left(1-\nu, \frac{\nu\mu_0+\bar{\tau}}{\gamma_1\mu_0\bar{\tau}}\right)\right] \\ &= 1 - R_\Gamma \end{aligned} \tag{A.5a}$$

where

$$\mathcal{G}(1-\nu, x) = e^x \Gamma(1-\nu, x) \tag{A.5b}$$

in which $\Gamma(1-\nu, x)$ is the incomplete gamma function. For a diffuse source, these expressions become

$$\begin{aligned} t_\Gamma &= \left(\frac{\nu}{\gamma_1\bar{\tau}}\right)^\nu \mathcal{G}\left(1-\nu, \frac{\nu}{\gamma_1\bar{\tau}}\right) \\ &= 1 - r_\Gamma \end{aligned} \tag{A.6a}$$

Thus, once T_Γ and R_Γ have been computed, negligible effort is spent computing t_Γ and r_Γ, just as with regular two-stream approximations.

Appendix B

Derivation of (16) and (17)

This appendix furnishes a derivation of (16) and (17) for a cloud split into two layers (extension to multiple layers is straightforward). Consider a cloud like that in Fig. 1 in which both layers are characterized by ν with the upper and lower layers having mean

optical depths of $\bar{\tau}_1$ and $\bar{\tau}_2$. The normalized probability density function of τ for the lower portion is

$$p_{\Gamma_2}(\tau) = \frac{1}{\Gamma(\nu)} \left(\frac{\nu}{\bar{\tau}_2}\right)^{\nu} \tau^{\nu-1} e^{-\nu\tau/\bar{\tau}_2}. \tag{B.1}$$

Now, irradiance onto the lower portion depends on overlying cloud extinction. Thus, assuming perfect vertical correlation of optical depth, when (B.1) is weighted by direct-beam irradiance, it becomes

$$p_{\Gamma_2^*}(\tau) = \frac{1}{\Gamma(\nu)} \left(\frac{\nu}{\bar{\tau}_2}\right)^{\nu} \tau^{\nu-1} e^{-\nu\tau/\bar{\tau}_2} [e^{-\tau(\bar{\tau}_1/\bar{\tau}_2)}] \tag{B.2}$$

which is not normalized. The normalization factor for (B.2) is

$$\int_0^{\infty} p_{\Gamma_2^*}(\tau)\, \mathrm{d}\tau = \left(\frac{\nu}{\nu + \bar{\tau}_1}\right)^{\nu} \tag{B.3}$$

which when applied to (B.2) results in

$$p_{\Gamma_2^*}(\tau) = \frac{1}{\Gamma(\nu)} \left(\frac{\nu + \bar{\tau}_1}{\bar{\tau}_2}\right)^{\nu} \tau^{\nu-1} e^{-\tau(\nu+\bar{\tau}_1)/\bar{\tau}_2}. \tag{B.4}$$

This is (16) for $n = 2$. By forcing (B.4) into the form of (B.1), it becomes

$$p_{\Gamma_2^*}(\tau) = \frac{1}{\Gamma(\nu^*)} \left(\frac{\nu^*}{\bar{\tau}_2^*}\right)^{\nu^*} \tau^{\nu^*-1} e^{-\nu^*\tau/\bar{\tau}_2^*} \tag{B.5}$$

which requires that

$$\nu^* = \nu \tag{B.6a}$$

and

$$\bar{\tau}_2^* = \frac{\nu\bar{\tau}_2}{\nu + \bar{\tau}_1} \leqslant \bar{\tau}_2 \tag{B.6b}$$

and this is (17) for $n = 2$.

Figure B1 shows an example of the impact that the transformation in (B.6) has on the density function of the lower layer.

Appendix C

Bounded cascade clouds

The cascade begins with a homogeneous slab with liquid water path $\bar{\mathscr{L}}$. Then, the slab is halved and with equal probability, one half is selected at random and an amount $f\bar{\mathscr{L}}$ is shifted from it to the other half making two slabs with $(1 \pm f)\bar{\mathscr{L}}$. These slabs are halved again and the shifting process is repeated but this time fractions fc are shifted. By the m^{th} cascade, fractions fc^{m-1} are being shifted among 2^m cells. On a log-log plot, the slope of the power spectrum of $\mathscr{L}$ approaches, from above, $2\ \log_2 c - 1$ as $m \to \infty$. For details, see Cahalan *et al.* (1994a).

For given values of f and c, the normalized discrete density function $p_m(\mathscr{L})$ produced on the m^{th} cascade is identical for all realizations though the same cannot be said for the sequence $\{\mathscr{L}_i \mid i = 1, \ldots, 2^m\}$. This means that for the approximate radiative transfer models used here, all realizations for a particular f and c yield the same fluxes, but fluxes based on full 3D radiative transfer will differ slightly from one realization to the next.

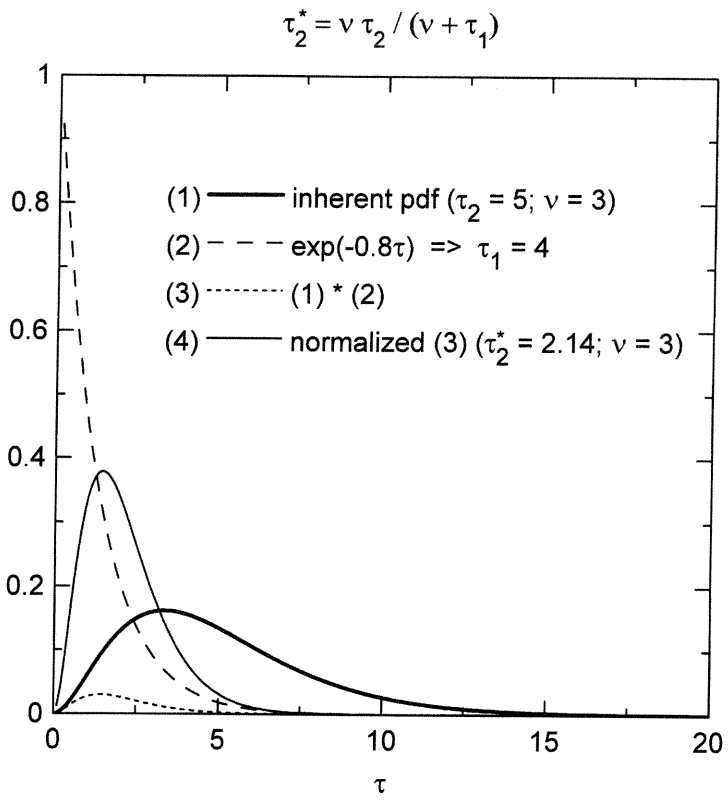

Figure B.1. Illustration of how the density function of optical depth of the lower portion of a two layer cloud is modified for normal incident direct-beam. The top layer has $\bar{\tau}_1 = 4$ and the lower portion has $\bar{\tau}_2 = 5$; both have $\nu = 3$. Curve (1) shows the inherent distribution for the lower layer; curve (2) is relative transmittance through the top layer; curve (3) is the product of (1) and (2) (i.e. Eq. B.2); and curve (4) is the renormalized effective density function for the second layer which is to be used when flux out the base of the top layer is assumed to be uniform.

The cascade model generates overcast clouds but non-overcast fields were produced as follows. Vertically-projected cloud fraction C is defined as

$$C = \sum_{\mathscr{L}_i > \mathscr{L}_{\text{crit}}} p_m(\mathscr{L}_i). \tag{C.1}$$

Once $\mathscr{L}_{\text{crit}}$ is found, $\mathscr{L}_i$ are reassigned as

$$\mathscr{L}_i \leftarrow \begin{cases} A(\mathscr{L}_i - \mathscr{L}_{\text{crit}}), & \mathscr{L}_i > \mathscr{L}_{\text{crit}} \\ 0, & \mathscr{L}_i \leqslant \mathscr{L}_{\text{crit}} \end{cases} \tag{C.2}$$

where A is a constant which forces the new mean of $\mathscr{L}_i$ to a desired value. Barker and Davies (1992) argued that this method may be credible if the original cascade is meant to represent some thermodynamic field related to the potential for cloud to exist and $\mathscr{L}_{\text{crit}}$ is a threshold above which conditions are conducive for cloud formation.

Figure C1 shows four histograms of $\mathscr{L}$ generated by the cascade model for $c = 0.794$, $m = 12$ and $\mathscr{L} = 50$ g m^{-2} along with corresponding $p_\Gamma(\mathscr{L})$ (discrete form; see Eq. (8) in Barker *et al.* 1996). For overcast conditions ($\mathscr{L}_{\text{crit}} = 0$), $p_\Gamma(\mathscr{L})$ capture the cascade distributions quite well. When $C = 0.5$, however, the modes that were present for overcast

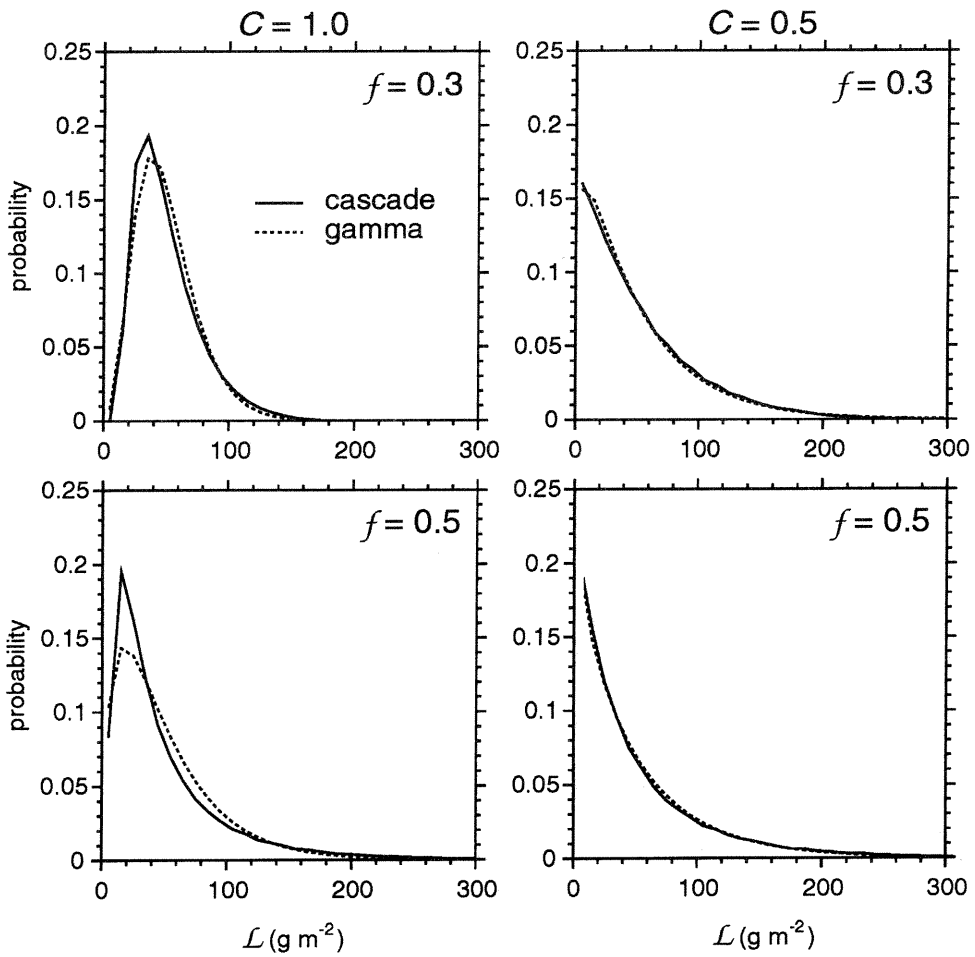

Figure C.1. Histograms of liquid water path $\mathcal{L}$ as predicted by the 1D bounded cascade model and the corresponding gamma distribution based on $\bar{\mathcal{L}}$ and $\overline{\ln \mathcal{L}}$ from the cascade model (see Eqs. (10) and (11)). Histograms are for two values of the cascade parameter f and two values of cloud fraction C.

$p_m(\mathcal{L})$ are truncated leaving just the tails which are described almost perfectly by $p_\Gamma(\mathcal{L})$ whose values of ν are smaller than those for the overcast cases. Truncating the fields at some $\mathcal{L}_{\text{crit}}$ as described in (C.1) effectively shifts the original $p_m(\mathcal{L})$ to the left and stretches it horizontally. The fact that ν for the truncated fields are almost always near 1.0 indicates that their tails are close to exponential.

Figure C2(a) shows ν (computed by Eq. (11)) for $f = 0.3$ and 0.5 as functions of C. Figure C2(b) shows the corresponding curves

$$\nu_{\text{clr}} = \frac{\nu C}{1 + \nu(1 - C)} \tag{C.3}$$

which are approximately the value ν would take if the clear-sky portion was used in its determination (this follows from the method of moments not MLE). Also plotted on both graphs are MLE estimates of ν and ν_{clr} for 42 of the 45 Landsat scenes used by Barker *et al.* (1996). The agreements between the Landsat-inferred values of ν and ν_{clr} and those

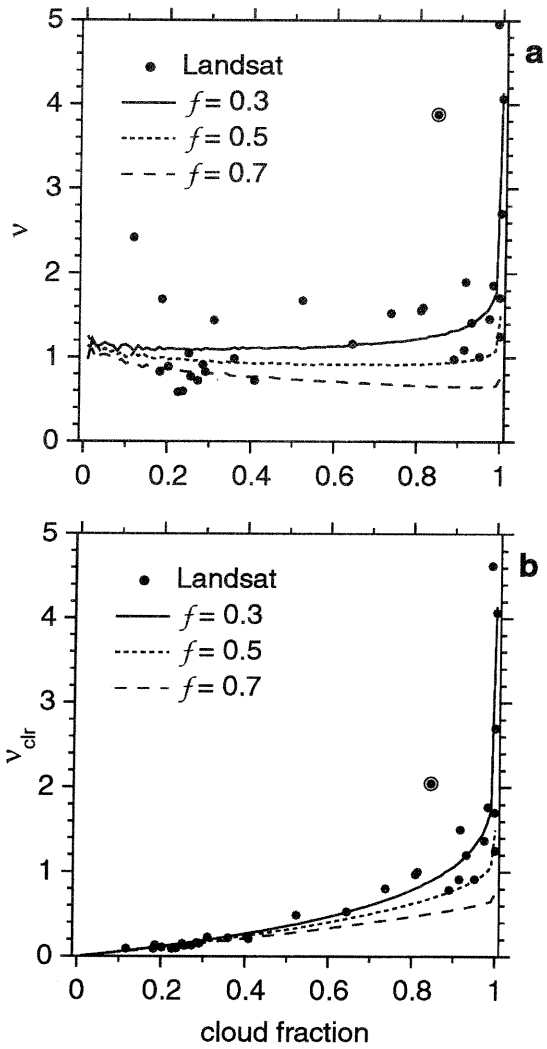

Figure C.2. (a) Dots represent MLE-based values of ν for the Landsat scenes of MBL clouds used by Barker *et al.* (1996) as a function of cloud fraction. The dot enclosed in a circle corresponds to a scene that had ~18% clear-sky confined to one corner. Thus, this field's value of ν is more suited to overcast conditions. Lines correspond to ν for the cascade model at different values of f (fields truncated as described in the text). (b) As in (a) except this is for ν_{clr} as defined in (C.3). To facilitate plotting, several values of $\nu = \nu_{\text{clr}} > 5$ for overcast scenes were not shown.

from the truncated bounded cascade model are surprisingly good; particularly for $f = 0.3$ where even the rapid reduction from $\nu \approx 4.2$ at $C = 1.0$ to $\nu \approx 1.8$ at $C = 0.99$ is captured well.

References

Alexander, G. D. 1995 The use of simulations of mesoscale convective systems to build a convective parameterization scheme. Ph.D. dissertation, Colorado State University

Barker, H. W. and Davies, J. A. 1992 Solar radiative fluxes for stochastic, scale-invariant broken cloud fields. *J. Atmos. Sci.*, **49**, 1115–1126

Barker, H. W. and Li, Z. 1995 Improved simulation of clear-sky solar radiative transfer in the CCC-GCM. *J. Climate*, **8,** 2213–2223

Barker, H. W. 1996 A parameterization for computing grid-averaged solar fluxes for inhomogeneous marine boundary layer clouds. Part I: Methodology and homogeneous biases. *J. Atmos. Sci.*, **53,** 2289–2303

Barker, H. W., Wielicki, B. A. and Parker, L. 1996 A parameterization for computing grid-averaged solar fluxes for inhomogeneous marine boundary layer clouds. Part II: Validation using satellite data. *J. Atmos. Sci.*, **53,** 2304–2316

Barker, H. W. and Wielicki, B. A. 1997 Parameterizing grid-averaged longwave fluxes for inhomogeneous marine boundary layer clouds. *J. Atmos. Sci.*, **54,** 2785–2798

Barker, H. W., Morcrette, J.-J. and Alexander, G. D. 1998 Broadband solar fluxes and heating rates for atmospheres with 3D broken clouds. *Q. J. R. Meteorol. Soc.*, **124,** 1245–1271

Briegleb, B. P. 1992 Delta-Eddington approximation for solar radiation in the NCAR Community Climate Model. *J. Geophys. Res.*, **97,** 7603–7612

Cahalan, R. F., Ridgway, W., Wiscombe, W. J., Bell, T. L. and Snider, J. B. 1994a The albedo of fractal stratocumulus clouds. *J. Atmos. Sci.*, **51,** 2434–2455

Cahalan, R. F., Ridgway, W., Wiscombe, W. J., Gollmer, S. and Harshvardhan 1994b Independent pixel and Monte Carlo estimates of stratocumulus albedo. *J. Atmos. Sci.*, **51,** 3776–3790

Chou, M.-D. 1992 A solar radiation model for use in climate studies. *J. Atmos. Sci.*, **49,** 762–772

Coakley, J. A., Jr., and Chýlek, P. 1975 The two-stream approximation in radiative transfer: Including the angle of the incident radiation. *J. Atmos. Sci.*, **23,** 409–418

Davis, A., Gabriel, P., Lovejoy, S., Schertzer, D. and Austin, G. 1990 Discrete angle radiative transfer—Part III: Numerical results and applications. *J. Geophys. Res.*, **95,** 11 729–11 742

Edwards, J. M. and Slingo, A. 1996 Studies with a flexible new radiation code. I: Choosing a configuration for a large-scale model. *Q. J. R. Meteorol. Soc.*, **122,** 689–719

Fouquart, Y. and Bonnel, B. 1980 Computations of solar heating of the Earth's atmosphere: A new parameterization. *Cont. Atmos. Phys.*, **53,** 35–62

Fu, Q., Krueger, S. K. and Liou, K.-N. 1995 Interactions of radiation and convection in simulated tropical cloud clusters. *J. Atmos. Sci.*, **52,** 1310–1328

Gabriel, P. M. and Evans, K. F. 1996 Simple radiative transfer methods for calculating domain-averaged solar fluxes in inhomogeneous clouds. *J. Atmos. Sci.*, **53,** 858–877

Geleyn, J.-F. and Hollingsworth, A. 1979 An economical analytical method for the computation of the interaction between scattering and line absorption of radiation. *Cont. Atmos. Phys.*, **52,** 1–16

Henyey, L. C. and Greenstein, J. L. 1941 Diffuse radiation in the galaxy. *Astrophys. J.*, **93,** 70–83

Joseph, J. H., Wiscombe, W. J. and Weinman, J. A. 1976 The delta-Eddington approximation for radiative transfer. *J. Atmos. Sci.*, **33,** 2452–2459

King, M. D. and Harshvardhan 1986 Comparative accuracy of selected multiple scattering approximations. *J. Atmos. Sci.*, **43,** 784–801

Liou, K.-N. 1992 *Radiation and cloud processes in the atmosphere*. Oxford University Press, New York

Marshak, A., Davis, A., Wiscombe, W. J., Ridgway, W. and Cahalan, R. F. 1998 Biases in shortwave column absorption in the presence of fractal clouds. *J. Climate*, **11,** 431–446

McClatchey, R. A. Fenn, R. W., Selby, J. E. A., Volz, F. E. and Garing, J. S. 1972 'Optical properties of the atmosphere. 3rd edition'. AFCRL-72-0497 (NTIS N7318412)

McFarlane, N. A., Boer, G. J., Blanchet, J.-P. and Lazare, M. 1992 The Canadian Climate Centre second-generation general circulation model and its equilibrium climate. *J. Climate*, **7,** 1013–1044

Meador, W. E. and Weaver, W. R. 1980 Two-stream approximations to radiative transfer in planetary atmospheres: A unified description of existing methods and a new improvement. *J. Atmos. Sci.*, **37,** 630–643

Morcrette, J.-J. and Fouquart, Y. 1986 The overlapping of cloud layers in shortwave radiation parametrizations, *J. Atmos. Sci.*, **43,** 321–328

Oreopoulos, L. 1996 'Plane parallel albedo bias from satellite measurements'. Ph.D. thesis, McGill Univ., Montreal, Canada. Available as C2GCR report no. 96-10

Oreopoulos, L. and Davies, R.	1998a	Plane parallel albedo biases from satellite observations. Part I: Dependence on resolution and other factors. *J. Climate* (in press)
	1998b	Plane parallel albedo biases from satellite observations. Part II: Parametrizations for bias removal. *J. Climate* (in press)
Pielke, R. A., Cotton, W. R., Walko, R. L., Tremback, C. J., Lyons, W. A., Grasso, L. D., Nicholls, M. E., Moran, M. D., Wesly, D. A., Lee, T. J. and Copeland, J. H.	1992	A comprehensive meteorological modeling system – RAMS. *Meteorol. Atmos. Phys.*, **49,** 69–91
Ritter, B. and Geleyn, J.-F.	1992	A comprehensive radiation scheme for numerical weather prediction models with potential applications in climate simulations. *Mon. Weather Rev.*, **120,** 303–325
Schneider, S. H. and Dickinson, R. E.	1976	Parametrization of fractional cloud amounts in climate models: The importance of modelling multiple reflections. *J. Appl. Meteorol.*, **15,** 1050–1056
Slingo, A.	1989	A GCM parametrization for the shortwave radiative properties of water clouds. *J. Atmos. Sci.*, **46,** 1419–1427
Stephens, G. L.	1988a	Radiative transfer through arbitrary shaped optical media: Part I: A general method of solution. *J. Atmos. Sci.*, **45,** 1818–1836
	1988b	Radiative transfer through arbitrary shaped optical media: Part II: Group theory and simple closures. *J. Atmos. Sci.*, **45,** 1837–1848
Stephens, G. L., Gabriel, P. M. and Tsay, S.-C.	1991	Statistical radiative transfer in one-dimensional media and its application to the terrestrial atmosphere. *Trans. Theory Stat. Phys.*, **20,** 139–175
Stubenrauch, C. J., Del Genio, A. D. and Rossow, W. B.	1997	Implementation of subgrid cloud vertical structure inside a GCM and its effects on the radiation budget. *J. Climate*, **10,** 273–287
Tian, L. and Curry, J. A.	1989	Cloud overlap statistics. *J. Geophys. Res.*, **94,** 9925–9935
Tiedtke, M.	1996	An extension of cloud-radiation parametrization in the ECMWF model: The representation of subgrid-scale variations of optical depth. *Mon. Weather Rev.*, **124,** 745–750
Welch, R. M. and Wielicki, B. A.	1984	Stratocumulus cloud field reflected fluxes: The effect of cloud shape. *J. Atmos. Sci.*, **41,** 3085–3103
Wielicki, B. A. and Parker, L.	1994	'Frequency distributions of cloud liquid water path in oceanic boundary layer cloud as a function of regional cloud fraction'. Pp. 415–417 in *AMS Eighth Conference on Atmospheric Radiation*, Jan. 23–28, Nashville, TN
Wiscombe, W. J.	1977	The delta-Eddington approximation for a vertically inhomogenous atmosphere. NCAR Tech. Note, TN-121+STR
Yu, W., Garand, L. and Dastoor, A. P.	1997	Evaluation of model clouds at 100 km scale using GOES data. *Tellus*, **49A,** 246–262